Temperature-dependent evolution of the electronic and local atomic structure in the cubic colossal magnetoresistive manganite La$_{1-x}$Sr$_x$MnO$_3$

N. Mannella,[1,2,*] C. H. Booth,[3] A. Rosenhahn,[2,†] B. C. Sell,[1,2] A. Nambu,[2,4,‡] S. Marchesini,[2,§] B. S. Mun,[1,2,§]
S.-H. Yang,[2,∥] M. Watanabe,[2,5] K. Ibrahim,[2,6] E. Arenholz,[7] A. Young,[7] J. Guo,[7] Y. Tomioka,[8] and C. S. Fadley[1,2]

[1]*Department of Physics, UC Davis, Davis, California 95616, USA*
[2]*Materials Sciences Division, Lawrence Berkeley National Laboratory (LBNL), Berkeley, California 94720, USA*
[3]*Chemical Sciences Division, LBNL, Berkeley, California 94720, USA*
[4]*Department of Chemistry, The University of Tokyo, Tokyo 113-0033, Japan*
[5]*RIKEN, Hyogo 679-5148, Japan*
[6]*Beijing Synchrotron Radiation Laboratory, Beijing 100039, China*
[7]*Advanced Light Source, LBNL, Berkeley, California 94720, USA*
[8]*National Institute for Advanced Industrial Science and Technolog (AIST), Tsukuba Central 4, Tsukuba 305-8562, Japan*
(Received 1 May 2007; revised manuscript received 6 December 2007; published 27 March 2008)

We have studied the temperature-dependent evolution of the electronic and local atomic structure in the cubic colossal magnetoresistive manganite La$_{1-x}$Sr$_x$MnO$_3$ ($x=0.3-0.4$) with core and valence level photoemission (PE), x-ray absorption spectroscopy (XAS), x-ray emission spectroscopy (XES), resonant inelastic x-ray scattering (RIXS), extended x-ray absorption fine structure (EXAFS) spectroscopy, and magnetometry. As the temperature is varied across the Curie temperature T_C, our PE experiments reveal a dramatic change of the electronic structure involving an increase in the Mn spin moment from $\approx 3\mu_B$ to $\approx 4\mu_B$, and a modification of the local chemical environment of the other constituent atoms, indicative of electron localization on the Mn atom. These effects are reversible and exhibit a slow-time scale, with an ≈ 200-K-wide hysteresis centered at T_C. Based on the probing depths accessed in our PE measurements, these effects seem to survive for at least $35-50$ Å inward from the surface, while other consistent signatures for this modification of the electronic structure are revealed by more bulk-sensitive spectroscopies such as XAS and XES/RIXS. We interpret these effects as spectroscopic fingerprints for polaron formation, associated with the presence of local Jahn–Teller distortions of the MnO$_6$ octahedra around the Mn atom, as revealed by the EXAFS data. Magnetic susceptibility measurements, in addition, show typical signatures of ferromagnetic-cluster formation well above the Curie temperature.

PACS number(s): 71.38.−k, 71.30.+h, 75.47.Gk

I. INTRODUCTION

Hole-doped manganese oxides with the perovskite structure and formula unit $R_{1-x}A_x$MnO$_3$ (where R and A denote a trivalent rare-earth atom and a divalent atom, respectively) have received a great deal of attention because of their unusual electronic and magnetic properties.[1–5] These materials are termed *colossal magnetoresistive* (CMR) since they exhibit a negative magnetoresistance, in which the relative drop of the resistivity upon application of a magnetic field can be orders of magnitude greater than that achieved, for example, in magnetic multilayer structures of the giant magnetoresistive type.[6] The large CMR effect and the half-metallic ferromagnetic nature[7–9] of their electronic structure make the CMR materials suitable for applications such as magnetic sensors, magnetic storage devices, and spin injectors. In addition, model devices based on heterostructures with tailored magnetic and transport properties involving CMR thin films are currently under study.[10]

In addition to these technological applications, the CMR oxides have been intensively studied in the past few years because of the possibility of accessing different crystallographic and electronic phases by experimentally controlling external parameters such as temperature, pressure, and doping concentration. This possibility allows testing various theoretical models for the description of strongly correlated

electron systems, of which the CMR oxides are a prototypical example. A proper description of the physics of the CMR oxides requires a detailed understanding of the interplay between charge, spin, lattice, and orbital orientation degrees of freedom.

In spite of extensive study, the CMR oxides are still not fully understood and pose continuing theoretical and experimental challenges. The long-standing double exchange (DE) model provides a qualitatively correct description of the CMR effect and is commonly adopted as the main ingredient to explain the physics of the manganites.[11] However, it has been pointed out that the DE model alone cannot quantitatively account for the large magnetoresistance observed.[12,13] Several theoretical and experimental results suggest that more complex, although not necessarily mutually exclusive, mechanisms such as short-range-ordered Jahn–Teller distortions (JTD) in the local environment of the magnetic atom, with resulting electron localization and polaron formation,[12–16] charge and orbital ordering,[17] and phase separation,[5,18,19] are needed to quantitatively explain the properties of these materials.

Since the CMR effect exploits a magnetic phase transition between a low-temperature ferromagnetic metallic (FM) state and a high-temperature paramagnetic metallic (PM) state, a correct understanding of the electronic structure in the FM and PM states and its temperature-dependent evolu-

tion above the Curie temperature T_C, at which long-range magnetic order disappears, is of paramount importance for a correct understanding of the physics in CMR manganites. In order to provide a more complete description of the electronic, magnetic, and local atomic structure of a CMR material across such a ferromagnetic-paramagnetic phase boundary, we have applied temperature-dependent core and valence level photoemission (PE), x-ray absorption spectroscopy (XAS), x-ray emission spectroscopy (XES) and its close relative resonant inelastic x-ray scattering (RIXS), extended x-ray absorption fine structure (EXAFS) spectroscopy, and magnetometry to the $La_{1-x}Sr_xMnO_3$ system (LSMO, with $x=0.3$ and 0.4). A brief description of some of these data has appeared previously,[20,21] and here we amplify and extend the arguments and conclusions presented previously, including additional experimental results.

Although much studied as a prototypical CMR material, LSMO is still a rather controversial system. On the one hand, LSMO is commonly referred to as a "canonical" DE system, that is, capable of being described by the DE model alone, since it shows the largest one-electron bandwidth and, consequently, is expected to be less affected by electron-lattice coupling and Coulomb correlation effects.[1,4,22–25] On the other hand, based on the observation of a splitting of the Mn-O peak into two distinct peaks in a pair distribution function (PDF) analysis of neutron data,[16,26,27] it has been suggested that JTDs are present in LSMO. However, other authors who have investigated LSMO with neutron scattering have recently questioned these prior results, so that unanimous agreement is lacking concerning the local atomic structure in LSMO.[28,29]

The data that we will present here indicate a dramatic change of the electronic structure in LSMO as the temperature is increased through T_C. As revealed by the PE measurements, on crossing T_C, the Mn spin moment increases from $\approx 3\mu_B$ to $\approx 4\mu_B$, while the binding energy of the O, Sr, and La atoms increases, suggesting the presence of electron localization on the Mn atom. These effects, which are reversible and exhibit an ≈ 200-K-wide hysteresis centered at T_C, seem to survive for at least $35–50$ Å inward from the surface. Other signatures of this profound modification of the electronic structure are revealed by more bulk-sensitive spectroscopies such as EXAFS, XAS, and XES/RIXS. In particular, the EXAFS measurements indicate the presence of local JTDs of the constituent MnO_6 octahedra around the Mn atom above T_C, while the XAS data show a correlation between the presence of JTDs and the absence of the splitting in the preedge region. While our spectroscopic data are indicative of polaron formation, the magnetic susceptibility measurements further show typical signatures of ferromagnetic clusters forming above T_C and beginning at a temperature $T^* \cong 1.3T_C$.

II. EXPERIMENT

For $x=0.3$ and 0.4, LSMO is in a metallic state and a rhombohedral crystallographic phase for the full temperature range accessed by our measurements ($110 \leqslant T \leqslant 600$ K). A phase transition from a FM to a PM state occurs as the tem-

perature is raised above the Curie temperature $T_C \approx 365$ K.[30,31] For all measurements, we used high-quality single crystals grown by the floating-zone method, with details on growth conditions and characterization of the samples reported elsewhere.[31]

The PE, XAS, and XES data have been taken with the multitechnique spectrometer/diffractometer endstation[32] located on the elliptically polarized undulator beamline 4.0.2 at the Berkeley Advanced Light Source, which provided photons in the energy range $85–1400$ eV.[33] The PE, XAS, and XES spectra have been measured on single crystals which have been fractured at room temperature *in situ* at base pressures better than 2×10^{-10} torr, with the average surface plane being perpendicular to the [211] direction as identified by Laue diffraction. The exposed surfaces are crystalline, as verified by x-ray photoelectron diffraction,[34] but not atomically flat due to the absence of cleavage planes such as those found in the closely related layered manganites.[1,5] We choose this approach in order to avoid possible deviations from the ideal stoichiometry introduced by more conventional surface preparation methods such as thin-film deposition and/or sputtering or annealing cycles[35] which, however carefully done, can alter the surface composition and atomic structure.

The PE, XAS, and XES spectra have been excited with linearly *p*-polarized light. A Scienta ES200 electron analyzer was used to record the PE and XAS spectra, with the latter measured in the electron yield mode by collecting secondary electrons of ≈ 100 eV kinetic energy. The analyzer was fully corrected for detector nonlinearity effects according to a procedure described elsewhere.[36] In order to maximize the probing depth, the spectra were collected in normal emission, i.e., with the electron analyzer set perpendicular with respect to the sample surface. The XES spectra have been collected using a Scienta XES 300 grating spectrometer. The same spectrometer was used to record additional O K-edge XAS spectra in the more bulk-sensitive fluorescence-yield mode by integrating the x-ray emission signal of the O $2p \rightarrow$ O $1s$ transition. Additional information regarding the experimental geometries is shown in Fig. 1 of Ref. 21.

Bulk-sensitive EXAFS measurements were carried out on a polished single-crystal LSMO surface and collected at the Stanford Synchrotron Radiation Laboratory on BL 4-1 with a 4-pixel Ge fluorescence detector.[37] Fitting methods and most other experimental details are the same as in Ref. 15, except that a self-absorption correction was applied and a third cumulant was included in the fit.[38]

Magnetic susceptibility was measured using a Quantum Design magnetic properties measurement system with a high-temperature oven insert. The sample was contained in an evacuated quartz tube and held in place with a small amount of quartz wool. The data are corrected for the magnetization of the container. The magnetic field was set to 100 Oe.

III. RESULTS AND DISCUSSION

A. Photoemission spectra: General phenomenology

The spectra recorded in our measurements include both the valence-band (VB) region and various core levels from

Mn, O, La, and Sr atoms. The core spectra provide an element-specific look at composition, as well as electronic and magnetic states, and further allow monitoring the individual responses to temperature variations of all of the constituent atomic species.

In particular, we have focused on the temperature dependence of the Mn 3s core-level spectra in order to provide information on magnetic states. Such spectra exhibit the expected doublet due to a multiplet splitting of the binding energy (BE), a well-known effect in transition metals which can sensitively probe the local spin moment of magnetic atoms[39–41] and which has recently been analyzed for several CMR materials, although with lower energy resolution than in the present data.[42,43] on emitting an electron from the 3s core level, two final states for the Mn ion are possible, depending on the coupling of the remaining 3s electron with the electrons in the unfilled 3d shell. Such multiplets, which thus arise from the exchange coupling of the remaining core 3s electron with the net valence spin S_v of the emitter, provide a source of spin polarized photoelectrons, with the spin polarization being referenced to the emitter magnetic moment and not to any laboratory frame;[44] the dominant polarizations are indicated at the bottom of Fig. 1(a). The multiplet energy separation ΔE_{3s} can be qualitatively estimated from $\Delta E_{3s} = (2S_v + 1)J^{eff}_{3s,3d}$, where $J^{eff}_{3s\text{-}3d}$ denotes the effective exchange integral between the 3s and the 3d shells, after allowing for final-state intrashell correlation effects.[39–41] The multiplet energy separation, therefore, permits estimating the local magnetic moment or, in other words, the net spin of the emitter atom. This simple exchange-splitting interpretation of the 3s spectra in transition metal oxides is no longer complete as the number of electrons increases (as in the case of Cu and Ni oxides) and/or as the electronegativity of the ligand decreases, in which case charge-transfer final-state screening effects become important and can lead to additional spectral structures. Nonetheless, the Mn 3s spectra of Mn oxides have been found in prior work to be dominated by more simply interpretable exchange effects, with charge-transfer satellite structures possibly being present but with low spectral weight.[40,41]

In mixed valence manganites with formula unit $R_{1-x}A_x$MnO$_3$, according to the simplest ionic model, the valencies of O, La, and Sr atoms are −2, +3, and +2, respectively, so as to yield by electron counting an average valency for the Mn atom of $(1-x)$Mn^{3+}+xMn^{4+}=Mn$^{(3+x)+}$, corresponding to a Mn 3d^{4-x} configuration. It is also well recognized that the Mn 3d-derived electronic states are split via crystal field interactions into localized t_{2g} and delocalized e_g orbitals. With the further simplifying assumption that the e_g electrons are localized and, thus, interact with the 3s electrons as the t_{2g}, the Mn 3s spectra for our example of x=0.3 can, in principle, originate from either a linear combination of two doublets corresponding to 30% Mn^{+4} (S=3/2) (S=3/2) and 70% Mn^{+3} (S=2), namely, two doublets whose separations amount to $\Delta E^{4+}_{3s} = 4J^{eff}_{3s,3d}$ and $\Delta E^{3+}_{3s} = 5J^{eff}_{3s,3d}$ or from an average between the Mn^{3+} and Mn^{4+} spins, with a net valence spin S_v of the emitter (Mn in this case) given by $S_v = \frac{1}{2}(4-x)$, thus yielding $\Delta E_{3s} \approx [5-x] J^{eff}_{3s,3d}$ or $4.7J^{eff}_{3s,3d}$. In either case, the Mn 3s multiplet is, thus, expected to be sensitive to changes in the relative numbers

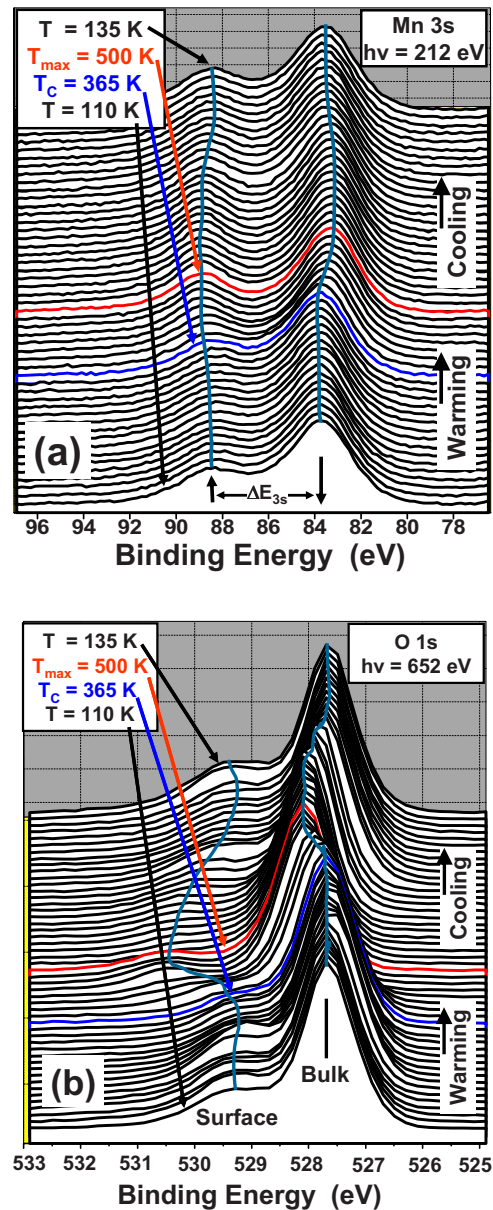
FIG. 1. (Color online) Temperature dependence of (a) Mn 3s spectra and (b) O 1s spectra from a freshly fractured surface of La$_{0.7}$Sr$_{0.3}$MnO$_3$. The photon energy indicated in each panel was chosen so as to yield the same inelastic mean free path ≈5–6 Å. The full dataset including heating and recooling was completed in about 24 h.

of Mn^{3+} and Mn^{4+} species that are thought to be present in these materials via the dependence of the peak separation ΔE_{3s} on the hole concentration x, as previously confirmed.[42,43] We stress, however, that it is only the localized Mn 3d character that will yield the full exchange interaction with Mn 3s, with the consequences of this being discussed further below.

In Fig. 1, we show a set of temperature-dependent core and valence photoemission spectra obtained in a single temperature scan on a sample of composition La$_{0.7}$Sr$_{0.3}$MnO$_3$ (x=0.3). The photon energy was set to 212.5 eV for the Mn 3s spectra [Fig. 1(a)], and 652 eV for the O 1s spectra [Fig. 1(b)] such that the O 1s photoelectrons have very
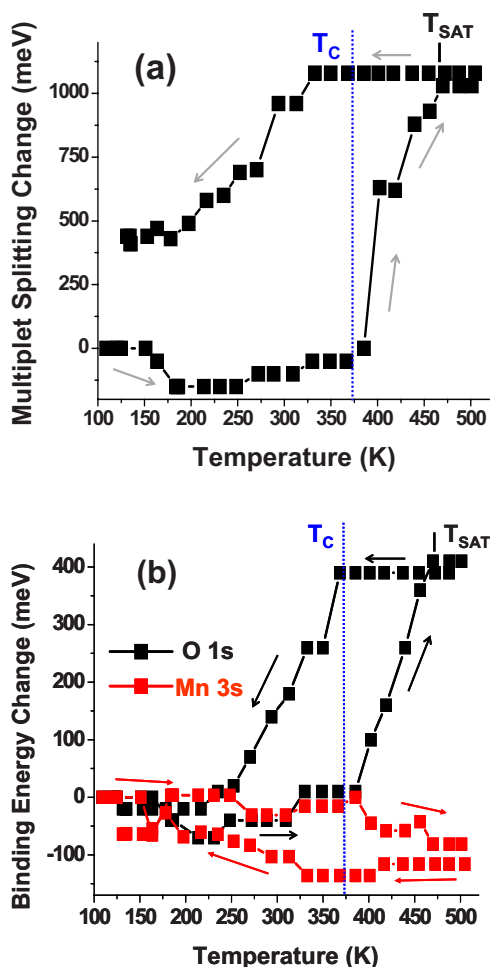
FIG. 2. (Color online) Temperature-dependent change of (a) the Mn $3s$ multiplet separation and (b) the O $1s$ BE and the weighted-average Mn $3s$ BE, as derived from the results in Fig. 1. Note the opposite direction of the BE shifts for the O $1s$ and Mn $3s$ core levels. The dotted blue line denotes the Curie temperature T_C.

nearly the same kinetic energy (and, thus, escape depth) as the Mn $3s$ electrons. The temperature range was 110–500 K, with a step of approximately 20 K. A full scan from low to high temperature and back again took about 24 h, with approximately equal time intervals for each step. In some experiments, more time (about 3 h) was spent at the maximum temperature to permit doing survey XPS scans and taking XAS, XES, and RIXS data, but the sample was observed in all scans to be very stable at this temperature and to return to its initial conditions and stoichiometry at the end of a scan.[45]

The Mn $3s$ splitting in Fig. 1(a) changes markedly, from 4.50 to 5.55 eV, as the temperature is raised from T_C to a higher "saturation" temperature $T_{sat} \approx 470$ K beyond which no change is observed. On cooling the sample in the same stepwise fashion, this splitting tends to return to its original value, but with an ≈ 200 K-wide hysteresis [Fig. 2(a)]. It was, furthermore, not possible to fit the Mn $3s$ spectra with a doping-weighted linear combination of two doublets corresponding to 30% Mn^{4+} ($S=3/2$) and 70% Mn^{3+} ($S=2$), namely, two doublets whose separations amount to $\Delta E_{3s}^{4+} = 4J_{3s,3d}^{eff} = 4.4$ eV and $\Delta E_{3s}^{3+} = 5J_{3s,3d}^{eff} = 5.5$ eV, where $J_{3s,3d}^{eff}$

≈ 1.1 eV as indicated by prior results from our and other groups for a range of inorganic Mn compounds.[40,41,43,46] On the contrary, it appears that the Mn $3s$ multiplets can be described in terms of a weighted sum between the Mn^{3+} and Mn^{4+} spins, thus yielding $\Delta E_{3s} \approx [5-x]J_{3s,3d}^{eff}$. This relationship between the multiplet separation and doping level x is generally well obeyed in the manganites.[42,43] When $x=0.3$, the value of the Mn $3s$ splitting is, thus, given by $\Delta E_{3s} = 5.17$ eV, which is at least in the range of our measured values. Interestingly, in a prior study of Mn $3s$ splittings in various CMR compounds,[43] the room-temperature value reported for the Mn splitting of 5.3 eV in La$_{0.7}$Sr$_{0.3}$MnO$_3$ lies between our two extreme values (4.4 and 5.55 eV), but is much closer to the high-temperature value of 5.55 eV. However, Fig. 1(a) indicates that this splitting should be much lower at room temperature, i.e., ≈ 4.4 eV, and this is a value we have reproduced over several samples. Besides the lower energy resolution used in this prior work,[43] some of this large discrepancy is most likely a result of the different modalities according to which experiments are performed, as for example, surface preparation and photon energy of excitation. Later we discuss the temperature dependence in Fig. 1(a).

Figure 1(b) shows O $1s$ spectra that were obtained simultaneously with those shown in Fig. 1(a), and again demonstrates significant changes with temperature on passing T_C. As we will further comment below, we have verified by changing the photon energy that the dominant low-BE O $1s$ peak in Fig. 1(b) is due to O atoms at greater depths below the surface,[45] and it is this "bulk" feature that we choose to analyze further. The bulk O-atom BE exhibits a sharp increase of about 400 meV on going above T_C, as well as hysteresis when the temperature is decreased, as shown in Fig. 2(b). These results are in qualitative agreement with the findings by Nylen *et al.*, who studied LSMO single crystals fractured in UHV and reported shifts toward lower BE for the O $1s$ bulk peak when samples were cooled from room to liquid nitrogen temperature.[47] While the O $1s$ BE loop closes on the time scale of our measurement, as shown in Fig. 2(b), the Mn loop does not [cf. Fig. 2(a)]; however, upon remaining at the lowest temperature for longer times (data not shown here), the Mn loop does eventually close, albeit on a slightly longer time scale (≈ 6–8 h). We attribute this difference to the additional collective magnetic character affecting the Mn $3s$ spectrum, perhaps due to ferromagnetic-cluster formation (as discussed further below), with this resulting in a slower time scale. Note also that the O $1s$ "surface" peak shows an even more dramatic shift on going to high temperature, but, as for the bulk feature, this returns to its initial position and shape on returning to low temperature.

Simultaneous with measuring the Mn $3s$ and O $1s$ spectra, O $1s$, La $4d$, La $5p$, Sr $3d$, Sr $4p$, and VB spectra were also recorded. The BEs of all of the O, La, and Sr core peaks were observed to increase by between 0.4 and 0.6 eV as the temperature was increased from T_C to T_{sat}, in parallel with the change of the Mn $3s$ splitting and the increase of the O $1s$ BE, further indicating a significant temperature-dependent change of the electronic structure. The increase of the core-level BEs for O, La, and Sr is not an artifact due to charging, as is unambiguously shown by the absence of any shift of the Fermi level (within the accuracy of our measurements) of

50 meV.[20,45] As shown in Fig. 1(b) of Ref. [20], the shape of the VB spectrum changes on going through T_C and reaching T_{sat}, with several features labeled $VB_1 - VB_4$ there showing significant temperature dependence and, similar to the O, La, and Sr core peaks, also reversibility with hysteresis. More specifically, the relative intensities of peaks VB_1 and VB_2 change somewhat, with the features VB_3 and VB_4 at higher BE showing much more pronounced shifts and changes in relative intensity; in fact, VB_3 is only weakly visible at low temperature.

By contrast, the weighted average of the BEs in the Mn 3s multiplet decreases slightly with increasing temperature [Fig. 2(b)], that is, in an opposite direction to the core shifts of all of the other chemical species. Although all of the results presented here are for $La_{0.7}Sr_{0.3}MnO_3$, we have seen identical effects in similar experiments on $La_{0.6}Sr_{0.4}MnO_3$, with the only difference being that T_{sat} does not occur until about 150 K above T_C. These phenomena are also not the result of artifacts due to surface contamination or alteration effects, but are indicative of an intrinsic and profound modification of the electronic structure occurring across the FM-PM phase boundary, a point that we now discuss below and which has been addressed more extensively elsewhere.[45]

B. Photoemission spectra: Surface characterization

As a first point, we note that all of the effects discussed so far are reversible and with slow hysteresis; moreover, measurements on samples immediately after fracturing and significantly later (approximately 1 day) in the same UHV environment yielded the same effects on crossing T_C. It is, thus, very unlikely that an adsorption or desorption phenomenon or surface composition change is responsible for the change in the electronic structure. Beyond these qualitative considerations, we have studied the surface composition of our samples by analyzing core-level intensity ratios, both as extracted from broad survey spectra and as taken over narrower energy ranges with higher energy resolution, smaller energy step, and better signal to noise ratio, which are reported in detail elsewhere.[45] Based on the results of these analyses, we can rule out temperature-dependent surface segregation or composition change and extrinsic contamination as a possible cause for the appearance of the effects discussed so far. In fact, the fractured surfaces studied here have routinely shown a high degree of cleanliness and stability in UHV, with XPS-determined surface compositions after fracture being the same as that of the nominal (bulk) stoichiometry to within experimental accuracy, and with minimal surface contamination or stoichiometry alteration with time, in contrast to what has been reported for certain CMR thin films.[35(c),35(d)] As one indicator of this, for the experiment which yielded most of the results described in this work, the C surface contamination was found to be between 0.035 monolayer (ML) just after fracture and 0.068 ML at the end of measurements. As another indicator, by measuring the ratio of the Sr 3d and La 4d intensities, we routinely extracted a value for the doping level $x = 0.3 \pm 0.02$ in samples with nominal doping value $x = 0.3$.

In addition to the use of core peak intensity ratios to directly determine sample stoichiometries and contaminant levels, another useful approach we used for surface characterization consists of comparing the temperature-dependent increase of the Mn 3s multiplet separation (the most important indicator of the change in electronic or magnetic state of the sample) with the temperature-dependent variation of the intensity ratios of several spectral features expressed as percentage changes and normalized to the low-temperature starting point.[45] These strictly empirical ratios do not involve any sort of theoretical input and should accurately mirror any subtle changes in relative intensity through a given temperature scan. The near constancy of the [Sr 4p]/[La 5p] ratio, to within about $\pm 6\%$ variation, not far from the expected error bars (as shown in Figs. 3(c) and 3(d) of Ref. [45]), is consistent with these two elements occupying the same average site types and with a negligible degree of surface segregation of one species or surface structural change as temperature is varied. We found that all of the similar ratios involving Sr 4p, La 5p, and Mn 3s core levels are confined to within small ranges of $\approx \pm 10\%$, and that they return within experimental error to their low-temperature values at the end of a cycle, thus suggesting that the near-surface composition of the LSMO is not significantly changed by this temperature excursion. Although such small changes may indicate some small variation in near-surface composition,[45] they can also be linked to small changes in atomic structure as temperature is raised, which could change the strong and different photoelectron diffraction effects that will occur for each of the peaks studied.[34]

As noted above, our data show the presence of additional "satellite" structures which appear on the high BE side of the O 1s peak [labeled surface in Fig. 1(b)] and in the high BE region of the valence spectra [VB_4 in Fig. 1(b) of Ref. [21]]. Some authors have identified these structures either as spectroscopic signatures of surface contamination[48] or surface modification such as surface segregation effects and/or oxygen desorption in UHV[47,49] Our data unambiguously show that the high-BE O 1s peak and the structure in the VB located at 9.5–10 eV are indeed due to atoms located in the outermost layers of the surface. In fact, these structures are much less pronounced at higher kinetic energy (KE) (and, thus, larger escape depth) of the photoelectrons, as shown by the O 1s and VB spectra taken at higher photon energies.[45] Even though oxygen desorption in UHV is, in general, a possible phenomenon at higher temperatures, our data seem to rule it out as a more plausible cause for the presence of the features in question. This is shown, for example, by the surface-associated O 1s peak at higher BE, exhibiting similar hysteresis to the bulk peak at lower BE [Fig. 1(b)]. These structures appeared in our experiments immediately after fracture and exhibit reversibility with temperature cycling, a behavior which is not compatible with the occurrence of O adsorption and/or desorption phenomena. As a matter of fact, though always present in our data, these structures are lower in intensity at higher temperatures, where O desorption is more likely to take place.[45] We estimated the surface coverage in ML associated with the O 1s surface peak by considering it as originating from a nonattenuating layer of O atoms sitting on or chemisorbed onto the surface.[45] This calculation yields an estimate for the quantity of this nonattenuating layer ranging from 0.35 ML at low temperatures to

0.24 ML at high temperatures. Since the high-BE O 1s surface peak originates from atoms located in the outermost layer, these atoms are not necessarily bound to Mn atoms or at least not in the same configuration as within the bulk. The more relevant [O 1s bulk]/[Mn 3s] ratio [cf. Fig. 10(b) in Ref. 45] varies from +8% to 15%, a range of 23%. Even though these numbers might at first seem to indicate O desorption related to the bulk peak of $\approx$15% at the highest temperatures, we note that in the temperature range 350–500 K, where the maximum change of the Mn 3s splitting takes place, the change in the ratio amounts to only $\approx$10% and, most importantly, it does not at all track with the change of the Mn 3s splitting. The kinetic energies being considered in this analysis are also low enough to yield a high surface sensitivity, with electron inelastic mean free path (IMFP) values expected to be in the 5–6 Å range.

In order to investigate further the potential impact of the small changes in peak ratios seen with temperature, we also considered the effects they might have on the Mn 3s splitting due to a deviation from the ideal surface stoichiometry. Most importantly, our analysis rules out the assumption that the increase of the Mn 3s splitting is caused by an increase of the Sr content with increasing temperature, as reported for the case of crystalline films.[35(c),35(d)] Indeed, a Sr-enriched surface would have the effect of *decreasing* the magnitude of the splitting because there would be more Mn^{4+} character. Our data, thus, strongly indicate that the high-T increase of the multiplet separation is not explicable by a change of the near-surface stoichiometry, and that the temperature-driven changes of the electronic structure are not artifacts due to surface contamination, adsorption and/or desorption phenomena, and/or surface segregation of the atomic constituents. More detailed discussions of all of these points appear elsewhere.[45]

C. Photoemission spectra: Electron localization effects

We now turn to the interpretation of the experimental PE results presented so far. The temperature dependence of the Mn 3s spectra suggests a significant increase in the Mn spin moment S_v at high temperature. The exchange interaction responsible for the 3s splitting is only nonzero when two wave functions overlap. Thus, $J_{3s,3d}^{\text{eff}}$, which is a per-electron number, should be constant with temperature and composition, but the overall splitting should in first approximation be directly proportional to the Mn 3d projected density of states, as converted into S_v in the above expressions, since the other components contributing to the t_{2g} and much more so the e_g states (e.g., O 2p, Mn 4s, and those with more plane-wave-like character) will overlap much less with Mn 3s. Our observed change in the Mn 3s splitting, thus, yields an estimate of an increase in the average Mn spin moment from $\approx$3μ_B to $\approx$4μ_B. Above T_C, the multiplet separation indicates the presence of a high spin state. In particular, the value of the magnetic moment extracted from the Mn 3s multiplet separation $\Delta E_{3s}=5.55$ eV for temperatures higher than $T_{\text{sat}}\approx$470 K is 4μ_B (i.e., $S=2$), somewhat higher than the nominal value for $x=0.3$ of 3.7μ_B ($S=1.85$), but rather close to the value 3.84μ_B ($S=1.92$) which results from a linear fit of inverse

magnetic susceptibility data for temperatures higher than T_{sat} as measured by our group on the same crystals used in the spectroscopy experiments, a point to which we will return below (cf. Sec. III G).

On the contrary, particularly intriguing is the value of the multiplet separation $\Delta E_{3s}=4.5$ eV below T_C, indicating that $S=1.5$, which is considerably lower than the nominal value $S=1.85$. If one considers the possibility that below T_C the Mn^{3+} ions can be found in a low spin state, namely, with a configuration t_{2g}^4, the value of the spin would be $S=1$, so that the value $S=1.5$ extracted from the multiplet separation $\Delta E_{3s}=4.55$ eV could be the result of a superposition of a low spin state $t_{2g}^{3.7}$ and a high spin state $t_{2g}^3 e_g^{0.7}$.

Rather, the variation with temperature of the Mn 3s separation and the variation of the BEs of La, Sr, and O suggests a profound change of the degree of covalency, namely, from a more covalent to a more ionic character at low and high temperatures, respectively. Thus, we find that it is easier to rationalize our findings by explaining the increase of the magnetic moment from 3μ_B to 4μ_B as a signature of an electron localization process. The e_g electron, fully delocalized at low temperature and with charge shared with the neighboring O, La, and Sr atoms, is more localized onto the Mn atom for temperatures higher than T_C, thus effectively increasing its exchange interaction with the 3s electrons and therefore assisting in increasing the splitting of the Mn 3s multiplet. The high-T increase of the core BEs for the O, La, and Sr core levels indicates a marked change of the chemical environment of these constituent atoms, which is further suggestive of a process in which electronic charge is transferred from these atoms onto the Mn atom. The high-T increase of the core BEs for the O, La, and Sr is qualitatively consistent with this localization process, as also suggested by the increase of the Mn 3s splitting. If the e_g electron, with some charge being shared with the O, La, and Sr atoms, is transferred to and localized on the Mn atom, La, Sr, and O core electrons are indeed expected to experience a more positive environment and, therefore, be detected at higher BE. Consistent with this picture is also the observation that the weighted average of the BE of the Mn 3s multiplet decreases slightly with increasing temperature, suggesting that the Mn experiences a more negative environment [cf. Fig. 2(b)]. As a final important aspect of this different behavior of the BEs of Mn with respect to that of the other atoms, we have directly compared the Mn 2p and O 1s core levels recorded below and above T_C [cf. Figs. 8(a) and 8(b) in Ref. 45]. The high-temperature spectra exhibit a shift by about 0.70 eV toward lower BE for the Mn 2p spectra, while the shifts are about 0.1–0.3 eV toward higher BE for the O 1s peak and for all of the other core levels not shown, as suggested already by the measurements performed at lower photon energy with better instrumental resolution [cf. Fig. 1(b)]. This result further supports the idea that there is a significant charge transfer to Mn, thus lowering the Mn 2p binding energy, while the other elements lose charge, thus increasing their BEs.

According to the above-described scenario, the Mn valency in LSMO for temperatures well below T_C is thus predominantly Mn^{4+}, markedly different from the value $Mn^{3.3+}$ predicted by the most simple ionic model. In fact, the close
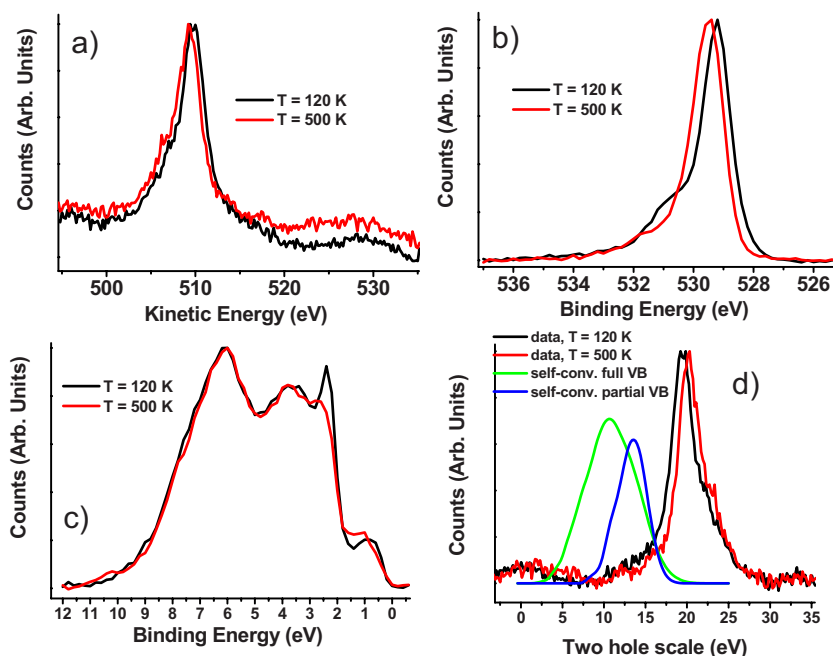
FIG. 3. (Color online) (a) O_{KLL} Auger spectra from $La_{0.7}Sr_{0.3}MnO_3$ recorded well below T_C (120 K, black line) and well above it (500 K, red line). The Auger spectra were excited with photons of 990 eV in order to avoid superpositions of the Auger peak with core-level photoelectron peaks. (b) O 1s core-level spectra recorded below and above T_C with a photon energy of 990 eV. (c) VB spectra recorded below and above T_C with photons of 950 eV, which should be approximately in the XPS (density of states) limit. (d) The Auger spectra below and above T_C plotted on the two-hole scale. Also shown are the SCDOS, as determined by using the whole VB spectrum (green line) and by using only that portion of the VB remaining after removing the Mn e_g and t_{2g} states (blue line). Note the increase of U (the distance between the center of the SCDOS and the Auger peak) for temperatures higher than T_C.

coincidence of the upper and lower values for the predicted and measured splittings (4.4 and 5.5 eV predicted for pure Mn^{4+} and Mn^{3+} configurations, and 4.50 and 5.55 eV observed at low and high temperatures) suggests a transition between a nearly pure Mn^{4+} spin state at lower temperatures and a nearly pure Mn^{3+} state at higher temperatures. Although somewhat surprising at first, this scenario is also supported by a recent self-interaction corrected local spin-density approximation calculation by Banach and Temmerman, which predicts that for $0.2 \leqslant x \leqslant 0.4$, the ground state of LSMO has a valency Mn^{4+}, while the Mn^{3+} ground state is preferred at higher temperatures as a consequence of the elongation of the MnO^6 octahedra.[50]

Further insights into this localization scenario are provided by the temperature dependence of the O core-valence-valence (CVV) Auger transition (O_{KLL}). In the absence of any correlation effects, if E_{VB}^1[1] and E_{VB}^2[2] denote the BEs of two electrons in the VB, the KE of the Auger electron is given by KE=$E_C - E_{VB}^1 - E_{VB}^2$,[2] where E_C denotes the BE of the core level involved, which is O 1s in this case. The maximum KE of a CVV Auger transition in a metallic system should thus be equal to the Fermi-referenced BE of the core level, since $E_{VB}^1 \approx E_{VB}^2 \approx 0$. Moreover, the line shape of the CVV Auger transition is expected to be given by the self-convolution of the density of states, as first recognized by Lander[51] Beyond this, the effect of the correlation of the two holes in the final state is to reduce the maximum KE of the CVV Auger transition by a quantity U and possibly to distort the spectral line shape.[52,53] As shown in Fig. 3(a), the Auger peak, measured with photons of 990 eV, indeed shifts toward

lower KE for temperatures higher than T_C. This behavior is particularly interesting when compared to the shift toward higher BE of the O 1s peak for temperature above T_C, as shown in Fig. 3(b) (cf. also Fig. 1). In order to resemble the density of occupied states, the VB was measured with a high photon energy of 950 eV, corresponding to the so-called XPS or density-of-states limit [Fig. 3(c)]. The states located at ≈ 0.8 and ≈ 2.5 eV correspond to the Mn e_g and t_{2g} states, respectively, as identified by resonant PE[49,54] We note that, at high T, there is a shift of the average of the full VB spectrum to higher BE, at least over the region from 0 to 4 eV binding energy, which is at least qualitatively consistent with the changes in the VB as seen with soft x-ray excitation [cf. Fig. 1(c) of Ref. 20], with these prior data expected to be selective to some specific region of the Brillouin zone (the ultraviolet photoemission spectroscopy limit). The self-convolutions of the full VB spectra at the low and high temperatures shown are virtually indistinguishable as expected since the self-convolution operation washes out the slight differences between the two spectra. Since we are considering the O_{KLL} Auger line, the self-convolution of the VB has also been computed after subtracting the Mn e_g and t_{2g} states from the VB by using a linear background subtraction over the BE region 0–3 eV. The choice of different backgrounds is irrelevant for the scope of this analysis, since the details of the spectral shapes are washed out eventually by the self-convolution operation. The O_{KLL} Auger spectrum and the self-convolution of the density of states (SCDOS) as obtained considering the full VB and the partial VB without the Mn e_g and t_{2g} states are shown in Fig. 3(d) on a two-hole

energy scale, i.e., the difference between the O 1*s* core-level BE and the KE of the Auger spectrum. [Note that this energy scale effectively reverses the curves shown in Fig. 3(a).] As expected in strongly correlated materials, the Auger line shape does not resemble the SCDOS as calculated by either method. On the contrary, the Auger line and the center of the SCDOS are displaced by an amount equal to the on-site two-electron repulsion energy U.[53] In the case shown here, U is estimated to range between 6 and 8 eV approximately, that is, within the $U/W \cong 1$ limit, where W denotes the VB bandwidth. These results and the shape of the Auger lines are similar to those of other samples of different compositions that we measured as well as to what has been reported for polycrystalline samples.[55] Since the limit $U/W \cong 1$ seems to be unaffected by the temperature change, as suggested by the absence of any appreciable change in the Auger line shape as a function of temperature, the shift toward higher energy on the two-hole scale for temperatures higher than T_C could be ascribed to an increase of the interaction strength U between the two holes in the two-hole final state. Besides being further indicative of a change of the degree of covalency, from a more covalent character at low temperature to a more ionic character above T_C, these results are consistent with electron localization onto the Mn atom, with less electronic charge on the O site being, thus, available for screening the two holes in the Auger final state, resulting in an increase of the hole-hole interaction energy U.

D. Photoemission spectra: Depth distribution of the observed effects

So far, we have largely discussed spectra with the KE of the photoelectrons being ≈ 130 eV for the deeper core levels [Figs. 1(a) and 1(b)] and 190–210 eV for shallower core levels and valence band, which yield estimated IMFPs of $\Lambda_e \approx 5$–6 Å.[45] An important issue is, thus, to establish unambiguously whether the observed changes in the electronic structure affect only the outermost atomic layers or whether it also affects deeper layers and perhaps the bulk as well. As a first point, the transition for both $x=0.3$ and 0.4 compositions always starts at the known bulk T_C, suggesting that the strong perturbation of the electronic structure is not exclusively related to the LSMO surface.

To further explore the depth distribution of the effects we observe, we have chosen to access different probing depths by varying the escape depth of the photoelectrons through changing photon energies. Unfortunately, we were not able to take advantage of selectively varying the surface sensitivity in our photoemission spectroscopy spectra by using the well-established method of decreasing the take-off angle.[56] This is because the surfaces that we obtained by fracturing samples were not atomically flat, and their roughness prevented us from correctly estimating the take-off angle, which is a crucial parameter for this kind of analysis.

In separate experiments on samples with $x=0.3$, we have measured for a sample of composition $x=0.3$ the VB, the O 1*s*, and all the core levels with BE below 100 eV with photon energies tuned so as to yield photoelectrons with KE ≈ 900 eV and inelastic mean free paths ≈ 15 Å, which correspond to 3–4 cubic unit cells, while the temperature was varied in the 110–500 K range (with a step of approximately 20 K). The Mn 3*s* splitting and the BEs of all the other O, La, and Sr core levels mentioned previously showed qualitatively the same temperature-dependent behavior observed in Figs. 1 and 2, although with magnitudes which are reduced somewhat, providing unambiguous evidence that the effects that we have observed at lower photon energy do not occur exclusively in the outermost surface layers, but seem to survive at least over the first 30–50 Å inward from the surface, or roughly 6–10 unit cells, as extensively discussed elsewhere.[45] In addition, it was possible to measure the Mn 3*p* core-level spectrum, whose structure is affected by the presence of multiplets as well, even though the analysis is not as straightforward as in the case of Mn 3*s* spectra due to the nonzero orbital angular momentum in the initial state (i.e., a *p* rather than an *s* orbital).[39] The BE of the main peak in the Mn 3*p* spectrum [cf. Fig. 12(b) in Ref. 45], decreases by about 0.5 eV when the temperature is increased, consistent with the weighted average behavior of the Mn 3*s* spectra [Fig. 2(b)] and the Mn 2*p* spectra [cf. Fig. 8(a) of Ref. 45], again suggestive of a net increase of electron charge on the Mn atom. Although the temperature-dependent variation of the multiplet separation and the BEs of the O, La, and Sr core levels look qualitatively similar to those measured at lower photon energies, there are some differences that we now address. First, although the BEs of O, La, and Sr core levels increase by 400–500 meV, in full agreement with the measurements at lower photon energy shown in Fig. 1, the hysteresis loops for the BEs of these core levels do not close on the time scale of the measurement.[45] The second one consists of a different ratio between the two peaks of the Mn 3*s* spectrum, a difference which is due to a change from an adiabatic to a sudden photoemission regime as the kinetic energy of the photoelectrons increases.[46] Moreover, the magnitude of the temperature-dependent change of the multiplet separation for the Mn 3*s* spectra amounts to ≈ 700 meV, and it is thus only about 64% of that measured with photons of 212 eV [≈ 1100 meV, cf. Figs. 1(a) and 2(a)].

The fact that the hysteresis curves do not fully close in this higher energy more bulk-sensitive dataset can be easily explained by an experimental procedural difference: a compressed time scale of the higher-energy measurements resulting in some temperature jumps larger than those in the experiments shown in Fig. 1, with the available experimental time not permitting us to wait for true equilibrium.[57] Indeed, we found that the O 1*s* BE decreases by ≈ 100 meV in a time of 4 h at the end of the experiment, after the sample had been cooled down to ≈ 140 K, thus bringing into focus the importance of effects linked to the kinetics of the electronic-structural phase transition indicated by our data. This statement is further corroborated by some additional results, shown here in Fig. 4, and consisting of Mn 3*s* and O 1*s* spectra measured in the same experimental run as the spectra shown in Fig. 1 at the lowest and highest temperatures with photon energies equal to 1000 and 1400 eV, respectively. In this case, the KEs and the IMFPs of the photoelectrons from both levels were ≈ 900 eV and ≈ 15 Å, corresponding to roughly 3–4 unit cells. These two sets of data (Fig. 4) show the same temperature-dependent behavior as shown by the

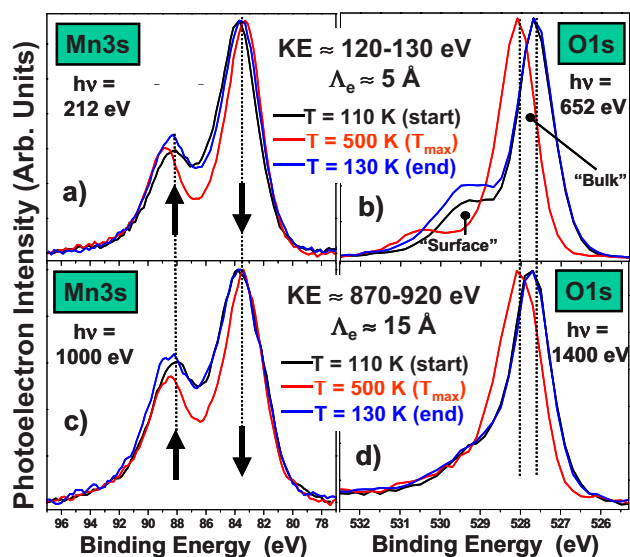FIG. 4. (Color online) Comparison of Mn $3s$ and O $1s$ spectra from La$_{0.7}$Sr$_{0.3}$MnO$_3$ recorded with low (120–130 eV) and high (870–920 eV) kinetic energies of the photoelectrons. The data were taken within the same experiment which provided the data shown in Fig. 1. The data have been recorded first at the beginning of the experiment (110 K), then at the maximum temperature of 500 K, and finally at the end of the experiment after the sample has been cooled down to 130 K. Note the marked difference between the intensity of the surface peak with respect to that of the bulk peak for the O $1s$ core-level spectra in (b) and (d).

spectra in Figs. 1(a), 1(b), and 3(b): at high temperature, the Mn $3s$ splitting increases and the O $1s$ binding energy increases. We note that the shoulder on the high BE side of the O $1s$ spectra is much less pronounced at the higher KE, indicating, as we have noted before, that this shoulder is related to O atoms near or on the surface. Because this peak is present immediately after fracturing the sample, does not track in any systematic way with the (very low) C contamination level, and has the same reversible behavior as the core peaks, we do not believe that it is connected with surface contamination or reaction. In this case, the values for the variation of the O $1s$ BE are nearly equal ($\approx$400 meV) for the spectra taken at low [652 eV, Fig. 4(b)] and high [1400 eV, Fig. 4(d)] photon energies. Moreover, the O $1s$ spectra taken at high photon energy [1400 eV, Fig. 4(d)] and recorded at low temperature at the beginning (110 K) and at the end (130 K) of the experiment are nearly identical and almost superpose perfectly [Fig. 4(d)]. This strongly suggests that when the temperature scans are performed according to the same modalities, the measurements with low and high photon energies yield the same results, at least for the O $1s$ spectra. The magnitude of the temperature-dependent change of the multiplet separation for the Mn $3s$ spectra in Fig. 4(c) amounts to $\approx$790 meV, which is $\approx$90 meV larger than that yielded by the data shown in Fig. 12(a) of Ref. 45 ($\approx$700 meV), and now 72% of the low-temperature result, again suggesting that the magnitude of the effects that we observe may also considerably depend on the time scale of the measurements. Nonetheless, the variation of the multiplet separation for the Mn $3s$ spectra is still considerably lower

than that shown in Figs. 1(a) and 4(a) ($\approx$1100 meV) for the spectra taken with a photon energy of 212 eV. We have systematically explored the possible effects on the multiplet separation caused by different inherent widths in the spectra due to the use of different instrumental resolutions while recording the spectra at low and high photon energies. Our analysis shows that the difference in the observed change in ΔE_{3s} between the spectra taken at low and high photon energies cannot be explained entirely in terms of a resolution difference alone. Nonetheless, the same analysis suggests that, although with magnitudes which may be reduced inward from the surface, the effects that we observed seem to survive at least over the first 30–50 Å inward from the surface (i.e., over the probing depth of the PE experiments), or roughly 6–10 unit cells, and therefore do not occur exclusively in the outermost surface layers.[45]

It is quite interesting that the effects related to the Mn $3s$ splitting show a stronger dependence on the probing depth than those affecting the other atoms. Moreover, while the BE loops of all the elements close on the time scale of the measurements shown in Figs. 1 and 2, the loop for the Mn $3s$ splitting does not, providing another peculiarity of the behavior of the Mn $3s$ splitting. Recent investigations of the temperature dependence of Mn $2p$ spectra from samples of the same composition carried out with photons of 7050 eV, with an attenuation length of $\approx$85 Å and hence yielding a much truer sampling of bulk properties, exhibit important differences with respect to the spectra shown in Fig. 8(a) of Ref. 45; these results will be reported elsewhere.[58] Although the general shape of the Mn $2p$ doublet is the same, the chemical shift with soft x-ray excitation of both Mn $2p$ components to higher BE on lowering the temperature to 150 K is much smaller and difficult to discern with hard x-ray excitation, thus suggesting that the effects seen in Fig. 8(a) of Ref. 45 are more localized near the surface. Another marked difference in the hard x-ray Mn $2p$ spectrum is the presence below T_C of a satellite peak which appears on the low BE side of the $2p_{3/2}$ peak, as already reported for other closely related manganite compounds.[59,60] This type of satellite has been interpreted as a nonlocal screening peak.[61] This satellite is also observed to slowly disappear as temperature is raised above T_C, thus indicating a temperature-dependent modification of the electronic structure taking place at greater depth than that of the effects discussed so far. It is thus possible that, rather than reflecting intrinsic differences between the surface and bulk properties of LSMO, the different effects seen in soft and hard photoemission experiments are indeed different signatures of the same phenomena caused by the different regimes accessed in the photoemission process. Indeed, additional bulk-sensitive XAS, XES, and EXAFS spectroscopy data to be discussed below indicate the presence of a modification of the electronic structure as the temperature is increased through T_C, with results that are consistent with the electron localization scenario suggested by our PE data.

E. X-ray absorption spectroscopy and x-ray emission spectroscopy–resonant inelastic x-ray scattering data

More bulk-sensitive XAS spectra (Figs. 11 and 12) measured over the O K and Mn L edges and detected with sec-

ondary electrons of ≈ 100 eV kinetic energy as well as photons in the fluorescence-yield mode show remarkable changes when the temperature is varied through T_C and up to T_{sat}. These results further indicate the presence of a drastic change in the electronic structure, which is not limited to the outermost surface layers.

The temperature dependence of the XAS spectra from our LSMO samples is remarkably similar to that reported by Toulemonde *et al.* for $Pr_{0.7}Sr_{0.3}MnO_3$ and $Pr_{0.7}Ca_{0.15}Sr_{0.15}MnO_3$ perovskites, as we have already discussed in particular for the O K-edge spectra.[21,62] In particular, the O preedge spectral region extending approximately 4 eV below the primary absorption threshold at ≈ 532 eV, which has received a great deal of attention since it represents the Mn $3d$-derived unoccupied states, is shown in Fig. 5(a) for three different temperatures. This spectrum was obtained using secondary electron detection. The presence of strong absorption in the preedge region reveals strong hybridization between the O $2p$ and Mn $3d$ states, thus indicating that the holes introduced upon doping with a divalent metal have a mixed Mn $3d$–O $2p$ character.[63] It is therefore not surprising that the profound change of the degree of covalency across T_C, as evidenced by the temperature dependence of the PE spectra, is also markedly visible in the XAS spectra. The most remarkable feature of the temperature dependence of the O K-edge XAS data is the disappearance of the double peak in the preedge structure, primarily through a loss of intensity of the peak located at 529 eV, for temperatures higher than T_C. Also noticeable is the suppression of a weak, but reproducible, structure at 531.5 eV for temperatures higher than T_C, as most clearly shown in the spectra collected in the fluorescence-yield mode [cf. Fig. 5(b)]. The spectra detected with secondary electrons and those collected in the more bulk-sensitive fluorescence-yield mode exhibit the same spectral features and the same temperature dependence, indicating that these effects cannot originate from the surface exclusively. The only difference between these two sets of data is that the structure at ≈ 531.5 eV is much more pronounced in the spectra collected in the much more bulk-sensitive fluorescence-yield mode, possibly as a consequence of using different detection methods, resulting in different matrix elements and fluorescence-yield effects. This structure is equally prominent in the fluorescence-yield spectra reported in Ref. 62. We interpret these O XAS data as a further signature of a charge transfer to the Mn atom for temperatures above T_C, as suggested by the loss of intensity of the lowest-energy structure located at 529 eV for temperatures above T_C.[21] Our results are thus in complete agreement with the $La_{0.7}Sr_{0.3}MnO_3$ data reported by Park *et al.*, who interpreted the disappearance of the splitting as a spectral weight transfer associated with the reduction of the density of the unoccupied $e_g^\uparrow$ states at the Fermi level at high temperatures,[64] an interpretation fully consistent with ours.

The interpretation of similar Mn L-edge spectra (Fig. 6) is not as straightforward as that of the O K-edge spectra, although we note that our data are remarkably similar to those reported by Toulemonde *et al.* on $Pr_{0.7}Sr_{0.3}MnO_3$ and $Pr_{0.7}Ca_{0.15}Sr_{0.15}MnO_3$ perovskites.[62] In particular, the shoulder at ≈ 638 eV in the L_3 edge loses intensity as temperature is decreased below T_C, a behavior which has been attributed
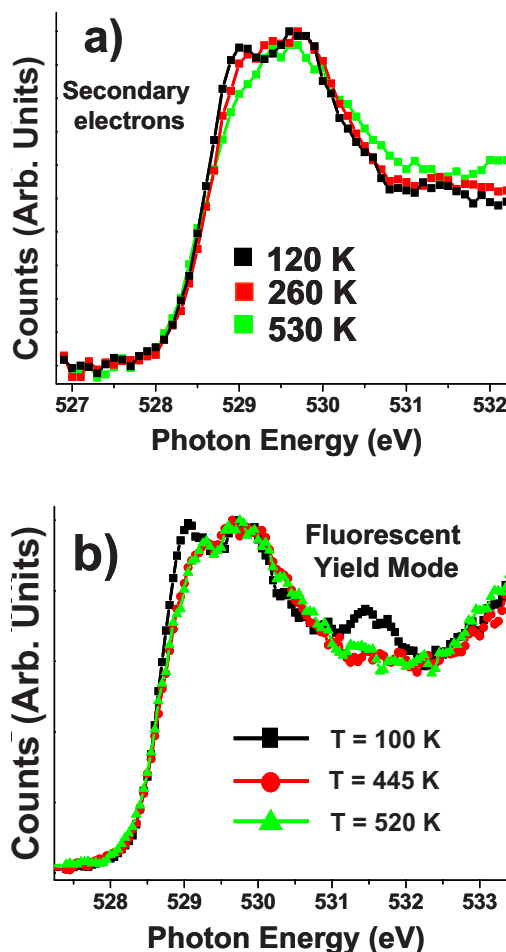

FIG. 5. (Color online) Temperature dependence of the preedge region in the O K-edge XAS spectra of $La_{0.7}Sr_{0.3}MnO_3$ detected (a) with secondary electrons of ≈ 100 eV kinetic energy and (b) in the fluorescence-yield mode. The double peak structure disappears for temperatures higher than T_C, which is a signature of polaron formation as proposed in Ref. 62. Note the similarity of the spectral features despite the fact that these spectra have been collected with secondary electrons in (a) and in the fluorescence-yield mode in (b), suggesting that these effects cannot be surface related. The spectra were recorded during the cooling-down cycle in (a) and the warming-up cycle in (b).

to an increase of the low-spin configuration in the absence of JTD.[62] Again, this is consistent with our interpretation of the PE data. The signatures of JTD in our XAS spectra will be discussed below.

Finally, the most bulk-sensitive XES and closely related RIXS data reveal a strong temperature dependence of the Mn $3d \rightarrow$ Mn $2p$ and O $2p \rightarrow$ O $1s$ transitions on crossing T_C and approaching T_{sat}, as shown in Fig. 7, again indicating the presence of a profound modification of the electronic structure which does not affect exclusively the outermost layer, but indeed more likely to be a bulk phenomenon. Figures 7(a) and 7(c) represent RIXS, in which the incident photon energy is positioned over a strong absorption resonance, whereas Figs. 7(b) and 7(d) represent simple XES, for which the incident photon energy is well above the relevant absorption edges. As shown in Figs. 7(a) and 7(b), there is a pro-
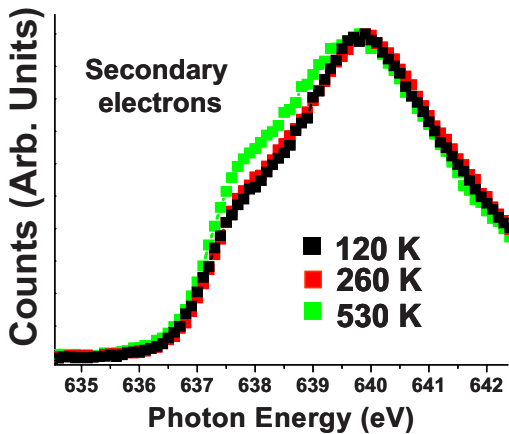
FIG. 6. (Color online) Temperature dependence of the *L*-edge region (Mn $2p_{3/2}$) in the Mn XAS spectra from La$_{0.7}$Sr$_{0.3}$MnO$_3$ detected with secondary electrons of ≈100 eV kinetic energy. Note the loss of intensity of the structure at 638 eV as temperature is decreased below T_C. The spectra were recorded during the cooling-down cycle.

gressive reduction of the width of the Mn RIXS and XES spectra as the temperature is increased above T_C, which is consistent with a more localized and thus narrower overall Mn $3d$ density of states. However, for the O RIXS and XES spectra shown in Figs. 7(c) and 7(d), width changes are less pronounced, and if anything are in the opposite direction,

with low-*T* spectra showing slightly narrower widths. Also different from Mn is that the O spectra exhibit a shift toward higher energies [Figs. 7(c) and 7(d)]. The most bulk-sensitive Mn and O spectra collected well above resonance [Figs. 7(b) and 7(d)] furthermore exhibit opposite shifts as a function of temperature, quite reminiscent of the shifts in opposite direction of the O $1s$ and Mn $2p$ core-level PE spectra [cf. Figs. 8(a) and 8(b) of Ref. 45]. That is, as the temperature is increased above T_C, the spectrum corresponding to the Mn $3d \rightarrow$ Mn $2p$ transition shifts to lower energies, while that for the O $2p \rightarrow$ O $1s$ transition shifts to higher energies. Although we are aware of the necessity of proper theoretical calculations to fully describe the hole states and line shapes involved, we note that the opposite directions of the shifts for the Mn and O XES spectra are at least qualitatively consistent with the shifts toward lower and higher BEs of the Mn $2p$ and O $1s$ core-level spectra, respectively.

F. Extended x-ray absorption fine structure

Our PE data have demonstrated a temperature-driven change of the electronic structure which is reversible and exhibits an ≈200-K-wide hysteresis centered at T_C with a time constant of several hours (cf. Fig. 2). This time dependence suggests that slow-relaxing atomic displacements are responsible for the perturbations of the core and valence levels. However, our samples are rhombohedral at all temperatures, and indeed no obvious fingerprints of a modification of
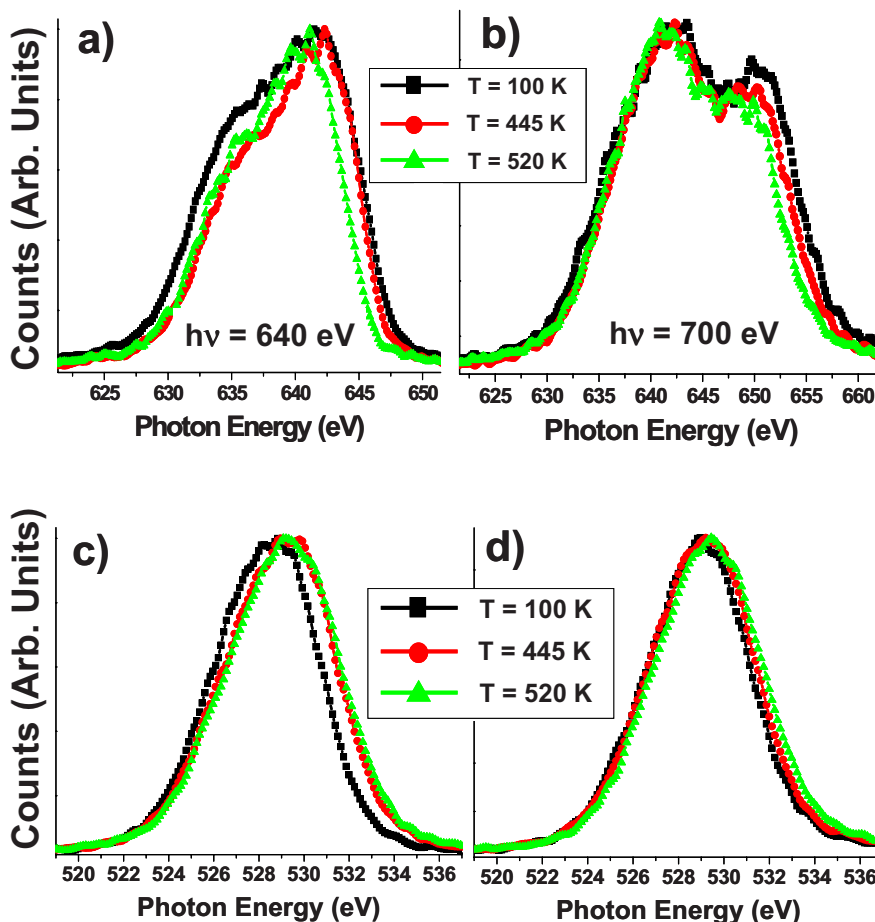

FIG. 7. (Color online) Temperature dependence of XES and RIXS spectra from La$_{0.7}$Sr$_{0.3}$MnO$_3$ corresponding to [(a) and (b)] the Mn $3d \rightarrow$ Mn $2p$ and [(c) and (d)] O $2p \rightarrow$ O $1s$ transitions, respectively. As temperatures go beyond T_C, there is [(a) and (b)] progressive reduction of the width of the Mn spectra and [(c) and (d)] a slight broadening and shift toward higher energies for the O spectra. Note how the most bulk-sensitive spectra collected well above resonance [(b) and (d)] exhibit the opposite shifts as a function of temperature, quite reminiscent of the shifts in the opposite direction of the O $1s$ and Mn $2p$ core-level PE spectra (see text).
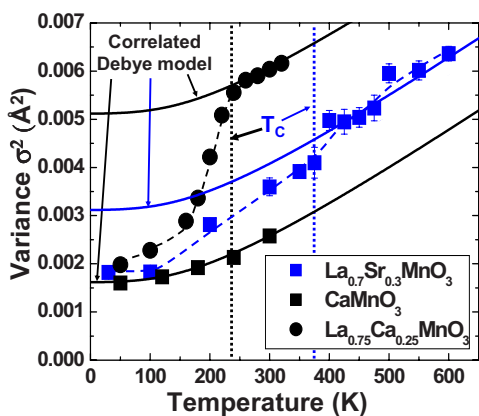
FIG. 8. (Color online) Variance σ^2 of the Mn-O bond length distribution in $La_{0.7}Sr_{0.3}MnO_3$ extracted from the bulk-sensitive EXAFS measurements at the Mn K-edge. Also shown for comparison are data from $La_{0.75}Ca_{0.25}MnO_3$, which is known to exhibit JTDs, and $CaMnO_3$, a JTD-free material. Also shown are three curves calculated within a correlated Debye model. Note that although the behaviors for LSMO and $La_{0.75}Ca_{0.25}MnO_3$ are qualitatively similar, the magnitude of the JTD in LSMO is only about half of that in the Ca-doped compounds.

the crystal structure are shown by x-ray crystallography over this temperature range.[31] It is thus possible that local, short-range-ordered modifications of the crystal structure occur on passing T_C. To investigate this possibility, bulk-sensitive Mn K-edge EXAFS measurements have been performed on a $La_{0.7}Sr_{0.3}MnO_3$ sample in the fluorescence-yield mode, with the temperature raised from 30 to 600 K. The EXAFS technique permits extracting the temperature dependence of the variance σ^2 of the Mn-O bond length distribution, as shown in Fig. 8. For temperatures well below and above T_C, σ^2 appears to have a gradual increase, consistent with a standard thermal broadening and described by the correlated Debye model, similar to that of the JTD-free $CaMnO_3$ material, which is also shown for comparison. However, as the temperature is increased toward T_C, σ^2 increases more rapidly than one expects from a vibrational analysis such as the correlated Debye model (solid curves).[65] The temperature dependence of the Mn-O bond length distribution width is qualitatively similar to a previous EXAFS study of $La_{1-x}Ca_xMnO_3$ (LCMO, $x=0.21$, 0.25, and 0.3),[15] one curve of which is shown in Fig. 8. The change in σ^2 with temperature for our LSMO sample is less dramatic than that for LCMO, but both show an onset near the respective Curie temperatures. These data thus provide experimental evidence that the lattice distortions observed above T_C are due to local John–Teller (JT) distortions around the Mn^{3+} ion. Our data thus suggest the occurrence of a JTD that develops with increasing temperature, saturating once the system becomes paramagnetic, as observed in $La_{1-x}Ca_xMnO_3$.[15] An interesting difference is that the apparent size of the JTD as inferred from σ^2 is only about half of that in the Ca-doped compounds. This difference may be the structural signature of the metallic state that survives in the paramagnetic state of the Sr-doped materials. Local JTDs and polaron formation have been observed by neutron scattering measurements with PDF analysis for LSMO up to $x=0.4$, although the magnitude of

the JTDs are larger than reported here.[16,26,27] However, our results are consistent with another recent EXAFS study.[66]

The presence of JTD is also suggested by the temperature dependence of the O K-edge prepeak structure (Fig. 5). The preedge structure extending from ≈ 528.5 to ≈ 530.3 eV can exhibit a double peak whose disappearance has been discussed by some authors as a signature for the presence of JTDs.[62] In fact, the suppression of the splitting of the oxygen preedge peak at ≈ 529–530 eV when the temperature is raised above T_C may be an indication of the unfolding of the unoccupied Mn $3d$ $e_g^\uparrow$ and $t_{2g}^\downarrow$ levels as a consequence of the symmetry breaking caused by the JTD, as first suggested by Toulemonde *et al.*[62] The same temperature-dependent presence or absence of the O preedge splitting has also been observed by our group for $La_{1-x}Ca_xMnO_3$, a system for which an unambiguous evidence for the presence of local JTD and polaron formation has been reported.[21]

We thus regard our results as spectroscopic signatures for the formations of JT polarons in the paramagnetic phase above T_C as predicted by Millis *et al.* in LSMO for $x>0.2$, with the JT energy remaining important even in the metallic state.[12,13] The occurrence of local JTD, as shown by the EXAFS measurements (Fig. 8), is in fact concomitant with the transfer to and/or localization of charge on the Mn atom. Evidence for this transfer or localization mechanism is provided by the observation for $T>T_C$ of the increase of the Mn $3s$ splitting and the opposite shifts to lower BE of the Mn $3s$ and Mn $2p$ core levels, and to higher BE of the O, La, and Sr core levels, respectively (cf. Figs. 1, 2, and 4). Moreover, the loss of intensity of the peak located at 529 eV and the consequent disappearance of the splitting in the O K-edge XAS prepeak structure in the paramagnetic phase (Fig. 5) are consistent with the presence of local JTDs and consequent polaron formation, as already suggested by Toulemonde *et al.*[62] In fact, the loss of intensity of the peak located at 529 eV can easily be explained by a reduction of the density of the lowest unoccupied states due to the electron localization above T_C associated with JTDs, and resulting reduced O $2p$–Mn $3d$ hybridization, an interpretation also consistent with the one provided by Park.[64]

We stress that, contrary to what is suggested by some as conventional wisdom, the presence of polarons and metallic conduction (our samples are always in a metallic phase) are not mutually exclusive, as already indicated by many theoretical works in polaron theory.[67] For the particular case of the manganites, neutron scattering measurements with PDF analysis have shown local JTDs in the metallic phases of $La_{1-x}Sr_xMnO_3$ up to $x=0.4$.[16,26,27] Similar results have been reported in a recent EXAFS study, even though the distortion in the metallic phase is observed to a lesser degree than in the PDF analysis.[66] Previous EXAFS studies have shown that below T_C, the polarons are not completely delocalized in $La_{1-x}Ca_xMnO_3$ as well.[15] Louca and Egami have discussed some of the possible mechanisms for the coexistence of metallic conduction and polarons, with the JT distorted regions being considered as regions which can spatially confine carriers, sometimes localizing them (insulating phase) and sometimes scattering them (metallic phase).[27] For our samples, the resistivity in the metallic state is high even at low T (≈ 100 $\mu\Omega$ cm below 100 K), indicating a strong scat-

tering of charge carriers in the metallic state, with the local distortions discussed above possibly being the source of such strong scattering.

G. Photoemission and magnetic susceptibility data: Phase separation and cluster states

In the past few years, some theoretical evidence has suggested that the phase-separated texture of the manganites is a key ingredient for understanding the physics of the CMR effect, perhaps without the necessity of invoking localization mechanisms.[68,69] Other authors have suggested a possible presence of phase separation for the $La_{1-x}Sr_xMnO_3$ system as well. Louca and Egami proposed that charges might be partially confined by spin and lattice rearrangements resulting in microscopic separation of the charge-rich and charge-poor regions,[27] while Shibata et al. found that Sr clustering could give rise to structural inhomogeneities on the nanometer scale and could provide a mechanism for the nucleation of a larger scale phase separation.[70] The noticeable ≈200-K-wide hystereses centered at T_C in our PE data (cf. Fig. 2) are strongly indicative of a first-order phase transition with marked effects linked to the overheating and undercooling dynamics. In order to determine whether the change in electronic structure that we observe on crossing T_C is consistent with the occurrence of phase coexistence, we have first fitted the temperature-dependent Mn 3s and O 1s core spectra with a linear superposition of the spectra at low temperature (<200 K) and high temperature (≥ T_{sat}). The only free parameter used in the fit is the fraction f of the high-temperature spectrum. Some of the results of this type of fit spectra are shown in Fig. 9, which shows that there is indeed excellent agreement with experiment. By demonstrating that the spectra taken with $T_C < T < T_{sat}$ can be expressed as a linear combination of spectra acquired at low and high temperatures, these results thus suggest the coexistence of unique low- and high-temperature electronic states and are at least consistent with the presence of phase coexistence in these materials. However, our core-level measurements probe only the short-range electronic structure, and so do not provide any information on the sizes of the domains of these two phases.

Theoretical studies predict that the intrinsic phase separation at the nanoscale would be responsible for both the existence of a new temperature scale T^* and the presence of ferromagnetic clusters in the temperature range $T_C \lesssim T \lesssim T^*$, which would grow in size when the temperature is reduced toward T_C.[5,69] The presence of ferromagnetic clusters above T_C has also been proposed on the basis of arguments involving the existence of magnetic polarons.[14,71–74] Above T_C, the carriers become localized as the lattice is distorted and magnetically polarizes the neighboring Mn atoms, forming ferromagnetic clusters. Experimental evidence for the existence of such magnetic polarons has been reported for other closely related manganite compounds.[14,71,73] The mechanism of a temperature-driven ferromagnetic-to-paramagnetic phase transition would be equivalent to that proposed by De Teresa et al. for the case of a magnetic-field-driven transition:[14,71] decreasing the temperature through T_C re-

duces the carrier localization, enhancing the hopping of the carriers between different lattice sites. The number of ferromagnetic clusters decreases, but the spatial extension of the remaining clusters grows because the Mn magnetic moments become aligned on a longer order scale.

Because of the crucial importance that magnetic cluster formation might have on the physics of the CMR manganites, along with the lack of a unanimous agreement among the authors about the presence of magnetic polarons, it is interesting to ask whether our data can shed light on this important issue. An inspection of our spectroscopic results, yielded by techniques which provide information only on short-range length scales of the electronic structure, indeed reveals that our data are consistent with this description of a temperature-driven phase transition. The increase of the Mn 3s splitting (which sensitively probes the local spin moment of the Mn atoms) and the concomitant increase of the O, Sr, and La BEs are due to changes in the local magnetic state and chemical environment as the temperature is increased through T_C, with the loss of long-range order occurring at T_C but short-range order still possibly existing 50–100 K above the ordering temperature T_C up to the saturation temperature T_{sat}. In light of these considerations, it is interesting to address the possible relationship between the ferromagnetic transition and the polaron formation, and ask whether the saturation temperature T_{sat} can be identified indeed with the temperature at which cluster formation starts occurring, and thus also with the temperature T^* in Ref. 69. Susceptibility data provide further information on this issue.

Figure 10 shows the inverse magnetic susceptibility χ^{-1} extracted from magnetic susceptibility measurements on the same crystal used for the experiment shown in Fig. 1. Such measurements are, of course, bulk sensitive. The linear fit of the high-temperature portion of the data set permits extracting the value of the magnetic moment from the expression $\chi^{-1} = (T - \Theta)/C$, where Θ and C denote the paramagnetic Curie temperature and the Curie constant, respectively. For a collection of N atoms with spin S, the Curie constant is given by $C = (N\mu_B^2/3k_B)p^2$, with p^2 denoting the square of the magnetic moment $p^2 = 4S(S+1)$.[75] From the high-temperature fit of the data in Fig. 10, we obtained $\Theta = 389.2$ K and $C \cong 2.8$ emu K Mol^{-1}, thus yielding $p^2 = 22.4\mu_B^2$, which corresponds to a value for the spin $S = 1.92$. These values for S and p^2 are remarkably close to the values $S = 2$ and $p^2 = 24$ as extracted from the Mn 3s multiplet separation $\Delta E_{3s} = 5.55$ eV for temperatures higher than $T_{sat} \approx 470$ K [cf. Fig. 2(a)], and higher than the nominal value $p^2 = 21.3$ corresponding to the doping value $x = 0.3$. The temperature dependence of χ^{-1} starts deviating from the linear behavior predicted by the Curie–Weiss law for temperatures in the range 470–490 K, below which the behavior is roughly quadratic with a positive concavity, thus indicating an increase of the effective magnetic moment. We stress that this deviation from the linear Curie–Weiss-type behavior is not due to the onset of ferromagnetic correlations as typically observed in normal magnetic metals such as Fe or Gd for temperatures very close to T_C. Indeed, in this case, the deviation from the linear behavior takes place at remarkably high temperatures, of the order of $1.3T_C$, in fairly good agreement with similar measurements whose results have been interpreted as signa-
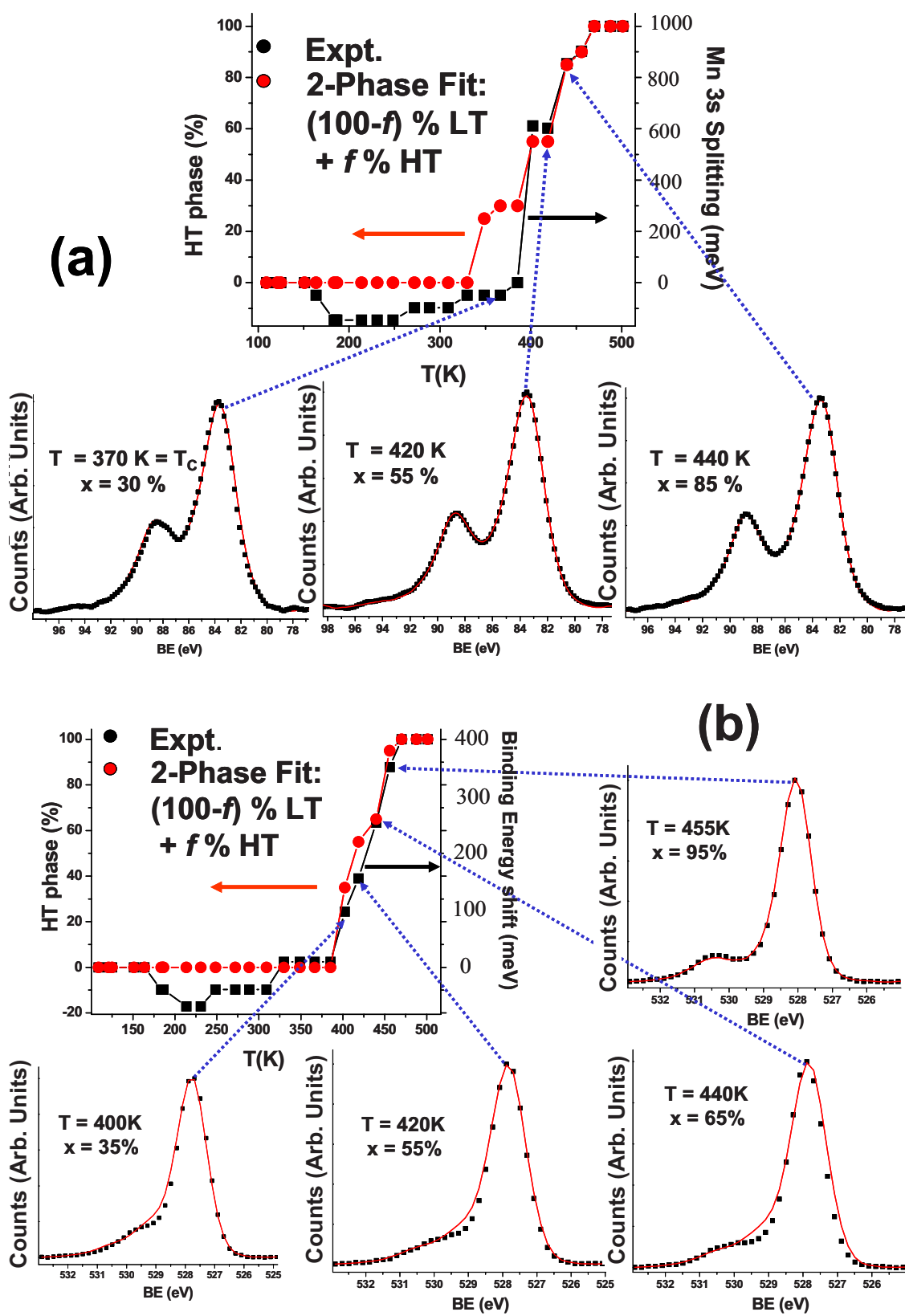
FIG. 9. (Color online) Two-phase fitting results for some (a) Mn 3*s* and (b) O 1*s* core-level spectra at different temperatures (cf. Fig. 1). The spectra have been fitted with a linear superposition of the spectra at low temperature ($<$200 K) and high temperature ($\geqslant T_{\text{sat}}$). The only free parameter used in the fit is the fraction f of the high-temperature spectrum. The possibility of expressing the spectra taken with $T_C < T < T_{\text{sat}}$ as a linear combination of spectra acquired at low and high temperatures suggests the coexistence of unique low- and high-temperature electronic phases and is consistent with the presence of phase coexistence in these materials.
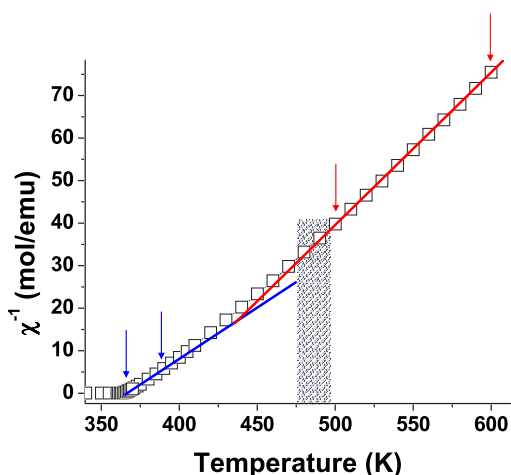
FIG. 10. (Color online) Inverse magnetic susceptibility extracted from magnetic susceptibility measurements on the same crystal used for the experiment shown in Fig. 1. The red and blue lines denote the fit to the curve for temperatures well above T_C (red) and approaching T_C (blue), while the red and blue vertical arrows indicate the range of data points used to yield the fits. The cross-hatched area marks the temperature below which significant deviation of the curve from the linear Curie–Weiss-type behavior begins to occur.

tures for the presence of magnetic clusters.[14,71,73] If a collection of N atoms is redistributed in clusters with an average number of n atoms per cluster, then the number of clusters and the square of the magnetic moment per cluster will be N/n and $p_{eff}^2 = (np)^2$, respectively, with the Curie constant given by $C = (N\mu_B^2/3nk_B)p_{eff}^2 = (N\mu_B^2/3k_B)np^2$, i.e., with an effective magnetic moment whose square value p_{eff}^2 is n times larger than that obtained in the Curie–Weiss regime. A linear fit of the data in Fig. 10 for temperatures very close to $T_C = 365$ K yields $C = 4.89$ emu K mol^{-1}, 1.75 times larger than the value obtained from the high-temperature fit, thus suggesting that the Mn ions for temperatures approaching T_C exist as dimers. Similar conclusions have previously been reached in an investigation of the La$_{0.7}$Ca$_{0.3}$MnO$_3$ ($x=0.3$) system, although the deviation from the linear Curie–Weiss behavior has been observed at higher reduced temperatures ($1.8T_C$).[73] Indeed, it is expected that in the presence of magnetic clusters, the effective moment derived from susceptibility measurements is larger than the value given by the nominal average of 0.7 Mn^{3+} and 0.3 Mn^{4+}.[72,74] Our magnetic susceptibility data thus show the existence of a temperature regime around $T \approx 470$–490 K, at which cluster formation starts occurring, and also suggest that we can identify the saturation temperature $T_{sat} \approx 470$ K revealed by the PE experiments with this temperature scale due to their remarkably similar values.

While the magnetic susceptibility data indicate an increase of the magnetic moment on approaching T_C, the PE measurements suggest that the Mn magnetic moment increases for increasing temperatures above T_C. These are not contradictory findings, since the PE measurements of the Mn 3s splitting yield the magnetic moment of the single Mn atom, while the susceptibility data provide information about the effective moment of magnetic clusters of atoms, with the
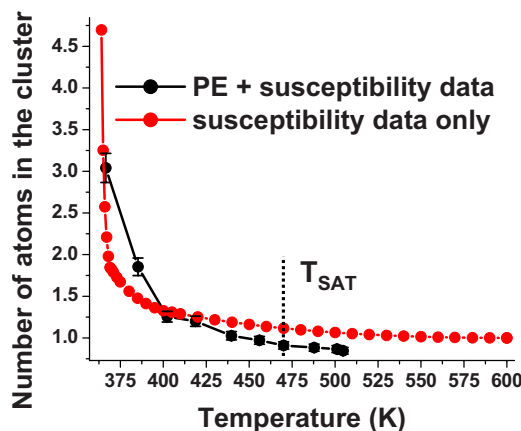

FIG. 11. (Color online) Average number of atoms in the clusters determined with the magnetic susceptibility data alone (red curve) and by combining the magnetic susceptibility data with the information provided by the analysis of the multiplet separation of the Mn 3s core-level spectra, as described in the text. When the latter is taken into consideration, the increase with temperature of the average number of atoms in the clusters upon approaching T_C from above is more gradual than what is suggested by the susceptibility data exclusively.

magnitude of the magnetic moment of single atoms being provided only in the Curie–Weiss limit at high temperatures. Taking into account both the susceptibility and the PE data, our findings suggest that the number of atoms in the clusters might be larger than the average number $n \cong 1.75$ as derived by analyzing only the susceptibility data.

In an attempt to provide a more complete picture of the temperature evolution of cluster formation across the ferromagnetic-to-paramagnetic transition, we have first calculated the variation with temperature of $p_{eff}^2(T)$ by fitting the χ^{-1} vs T curve shown in Fig. 10 with a high degree polynomial and then taking the first derivative of the resulting fit. We verified that using different polynomial degrees does not affect the determination of the first derivative, thus confirming the robustness of our procedure. When $p_{eff}^2(T)$ is divided by the value of p^2 derived from the linear fit of the χ^{-1} vs T curve at high temperatures, we obtain the temperature variation of the average number of atoms in the cluster $n(T)$ under the assumption that the magnitude of the atomic magnetic moment does not change with temperature (a simplification, since the PE data indicate that it does increase, by about $1\mu_B$, i.e., 33%), with the result shown in Fig. 11. We have then combined the magnetic susceptibility and the PE data in determining the average number of atoms in the clusters as a function of temperature by dividing $p_{eff}^2(T)$ by the values of $p^2(T)$ as derived from an analysis of the increasing-temperature portion of the multiplet separation of the Mn 3s core levels shown in Fig. 2(a). As shown in Fig. 11, the results of this approach suggest that, upon approaching T_C from above, the increase with temperature of the average number of atoms in the clusters is more gradual than what was suggested by the susceptibility data exclusively. We note, however, that this combination of bulk-sensitive susceptibility and more surface-sensitive photoemission results may, through the PE results, lead to more significant changes
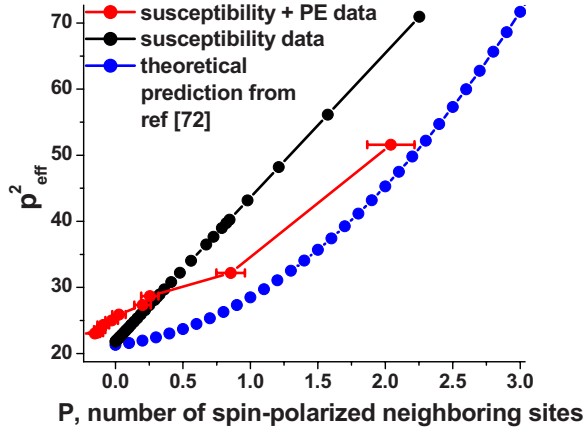
FIG. 12. (Color online) TThe variation of $p_{eff}^2(T)$ as a function of P, which is the number of spin-polarized neighboring Mn atoms. When the variation of the atomic magnetic moment $p(T)$ as derived from an analysis of the multiplet separation in the Mn $3s$ core-level PE spectra is taken into account, the variation of $p_{eff}^2(T)$ vs P (red curve) follows more closely the curve extracted from Eq. (1) of Ref. 72 (blue curve) than the straight line result obtained by considering the magnetic susceptibility data alone.

in moment than what really occurs in the bulk.

The possibility that the spins of the x Mn^{3+} and $(1-x)$ Mn^{4+} ions could effectively change as a result of the process of cluster or magnetic polaron formation has already been considered in the literature. If carriers become localized above T_C as the lattice is distorted and magnetically polarize a number P of neighboring Mn atoms, thus forming ferromagnetic clusters, we can express the square of the effective spin S_{eff} as[72]

$$S_{eff}^2 = x(S_1 + PS_2)(S_1 + PS_2 + 1) + (1 - x - Px)S_2(S_2 + 1),$$
(1)

where S_1 and S_2 denote the spins of the Mn^{4+} and Mn^{3+} ions, respectively. Since the number of atoms in the cluster is simply $n=P+1$, the variation of $p_{eff}^2=4S_{eff}^2$ as a function of P is markedly different from the linear behavior expected when the magnitude of the atomic magnetic moments is not allowed to vary. Interestingly, when the variation of the atomic magnetic moment $p(T)$ provided by the PE measurements is taken into account, the average number of atoms in the cluster is given by $n(T)=p_{eff}^2(T)/p^2(T)$, so that the variation of $p_{eff}^2(T)$ vs P follows more closely the curve extracted from Eq. (1), as shown in Fig. 12, thus suggesting that, in general, one has to take into account the possible temperature variation of the atomic magnetic moments to properly describe ferromagnetic-cluster formation.

A complete picture of the temperature evolution of cluster formation across the ferromagnetic-to-paramagnetic transition would necessarily require the evaluation of the expression $n(T)=p_{eff}^2(T)/p^2(T)$ for all of the temperatures accessed by the PE experiments of Fig. 1. It is significant that we have found that the magnetic susceptibility data do not show any hysteresis, not even when the temperature steps were changed in such a way that the whole magnetometry experiment would last as long as the PE experiments shown in Fig.

1, i.e., ≈ 24 h. This suggests that even though the effects shown by the PE measurements do not seem to affect only the outermost surface layers and despite the fact that other bulk-sensitive spectroscopies such as XAS, XES, and EX-AFS have detected signatures of a profound change of the electronic and local crystal structures, the magnetic properties in LSMO seem to exhibit different behaviors depending on the depth from the surface. Although it is plausible that strain effects may induce differences between the bulk and the first few hundreds of nanometers within the surface of LSMO, possibly resulting in different dynamics of the magnetic transition, at present we do not have a clear explanation for this particular aspect of our data, whose study should constitute the object of future stimulating investigations.

IV. CONCLUDING REMARKS

In conclusion, we have studied the temperature-dependent evolution of the electronic and local crystal structures in cubic colossal magnetoresistive manganites $La_{1-x}Sr_xMnO_3$ ($x=0.3-0.4$) with core and valence level PE, XAS, XES, RIXS, EXAFS spectroscopy, and magnetometry.

As the temperature is varied across the Curie temperature T_C, our PE experiments reveal a dramatic change of the electronic structure that is associated with an apparent increase in the Mn spin moment from $\approx 3\mu_B$ to $\approx 4\mu_B$ and an increase of the BEs of the O, Sr, and La atoms, indicative of a modification of the local chemical environment of these constituent atoms. The temperature-dependent changes in the Mn $3s$ splitting and in BEs are reversible and exhibit exhibit an ≈ 200-K-wide hysteresis centered at T_C with an hours-long time scale, indicative of a first-order phase transition. The possibility of expressing the Mn $3s$ and O $1s$ spectra taken with $T_C < T < T_{sat}$ as a linear combination of spectra acquired at low and high temperatures indicates the coexistence of unique low- and high-temperature electronic states, consistent with the presence of phase coexistence in these materials. However, our core-level measurements probe only the short-range electronic structure, and so do not provide any information on the sizes of the domains of these two phases. We have further shown that the effects seen in our data cannot be explained by a change of the near-surface stoichiometry, and that they are not artifacts due to surface contamination, adsorption and/or desorption phenomena, and/or surface segregation of atomic constituents. Rather, the effects revealed by our PE measurements are indicative of an intrinsic and profound modification of the electronic structure occurring across the FM-PM phase boundary. In light of these findings, we stress that the role played by different electronic and/or crystallographic phases have to be carefully taken into account when measurements of the type shown here are carried out in different portions of the phase diagrams, especially when data are recorded across a phase boundary.

We have interpreted our PE data as signatures of a localization of a Mn e_g electron onto the Mn atom as the temperature is increased above T_C. The e_g electron, fully delocalized at low temperature, is more localized onto the Mn atom above T_C, thus effectively increasing its exchange interaction with the $3s$ electrons, resulting in an increase of the Mn $3s$

splitting. The temperature behavior of the BEs of the constituent atoms supports this localization scenario. If the e_g electron, with some charge being shared with the O, La, and Sr atoms, is transferred to and localized on the Mn atom, La, Sr, and O core electrons are indeed expected to experience a more positive environment and therefore be detected at higher BE, as indeed observed in our experiments. The weighted average of the BE of the Mn $3s$ multiplet and the BE of the Mn $2p$ core level spectrum decreases slightly with increasing temperature, suggesting that the Mn atom experiences a more negative environment and is consistent with a significant charge transfer to the Mn atom. Our results strongly suggest that, in order to capture the complexity of the physics of the CMR oxides, it is thus necessary to abandon the most simplistic ionic model according to which the valencies of O, La, Sr, and Mn atoms are strictly 2^-, 3^+, 2^+, and $(1-x)Mn^{3+}+xMn^{4+}$, respectively. The inadequacy of this ionic model is also reflected by the presence of absorption in the preedge region of the O K-edge XAS spectra, which reveals strong hybridization between the O $2p$ and Mn $3d$ states, thus indicating that the holes introduced upon doping with a divalent metal have a mixed Mn $3d$–O $2p$ character, as already recognized by many authors.

Although the magnitudes of the PE effects we have observed may be reduced inward from the surface, the effects do not exclusively occur in the outermost surface layers. Based on the probing depths accessed in our PE measurements, these effects seem to survive for at least 35–50 Å inward from the surface, or roughly 6–10 unit cells, while other signatures indicative of a profound modification of the electronic and local crystal structures are revealed by more bulk-sensitive spectroscopies such as XAS, XES/RIXS, and EXAFS. Interestingly, we observed that when the temperature scans are performed according to the same modalities, the measurements with low and high photon energies yield the same results, at least for the O $1s$ spectra, bringing into focus the importance of effects linked to the kinetics of the electronic phase transition indicated by our data. We stress the importance of this point, which should not be overlooked, especially in the study of systems like the manganites which exhibit a pronounce instability toward different phases. In general, because of their first-order character, many phase transitions found in the manganites are expected to be strongly affected by overheating and undercooling dynamics, which is very sensitive to the kinetics and modalities of the experiments. Therefore, the details of the kinetics associated with a transition should be fully elucidated, in particular, in those cases in which experiments are indicative of phase coexistence, in order to unambiguously determine whether the latter is a fingerprint of the presence of phase separation or, more simply, an effect associated with the overheating-undercooling dynamics of the transition.

Our EXAFS measurements indicate the presence of local JTDs of the constituent MnO_6 octahedra around the Mn atom that develop with increasing temperature and then saturate once the system becomes paramagnetic. Our results are consistent with another recent EXAFS study and neutron scattering measurements with PDF analysis, although the magnitude of the JTDs for the neutron measurements is larger than reported here. Interestingly, the size of the JTD is only about half of that in the Ca-doped compounds, with this difference possibly being the structural signature of the metallic state that survives in the paramagnetic state of the Sr-doped materials.

We have interpreted our data as spectroscopic fingerprints of polaron formation, consistent with the presence of local Jahn–Teller distortions of the MnO_6 octahedra around the Mn atom as revealed by the EXAFS data and the localization of the Mn e_g electron as suggested by the PE measurements. Support for this scenario is also provided by the O K-edge XAS data, which show a correlation between the presence of JTDs and the absence of the splitting in the preedge region, a behavior which has already been observed in other systems for which an unambiguous evidence for the presence of local JTD and polaron formation has been reported.[21,62] By suggesting that polaron formation is a defining characteristic of the high-temperature paramagnetic state for the LSMO compounds, even when the electronic phase is metallic, our results assist in resolving the long-standing controversy of the presence of polarons in LSMO and thus challenge the division of the CMR materials into the two distinct canonical and noncanonical classes. Our results thus suggest that the presence of polarons above the Curie temperature is a general defining characteristic of all the CMR materials.

This work provides a description of the interplay between polaron formation and the ferromagnetic transition across the FM-PM phase boundary. In fact, our magnetic susceptibility measurements show typical signatures of ferromagnetic-cluster formation above T_C, occurring at a temperature T^* ≈ 470–490 K $\cong 1.3T_C$. Interestingly, the temperature T^* at which cluster formation starts occurring is remarkably close to the value of the saturation temperature $T_{sat} \approx 470$ K seen in the PE experiments, thus suggesting that T_{sat} and T^* could be identified with each other.

Finally, we have pointed out that, in general, one has to take into account the possible temperature variation of the atomic magnetic moments to properly describe ferromagnetic-cluster formation. Our approach of combining the magnetic susceptibility data and the analysis of the multiplet separation of the Mn $3s$ core-level PE spectra suggests that upon approaching T_C from above, the increase with temperature of the average number of atoms in the clusters is more gradual than what is suggested by the susceptibility data exclusively.

*Corresponding author. Present address: Department of Physics and Astronomy, University of Tennessee, Knoxville, TN 37996; nmannell@utk.edu

†Present address: Heidelberg University, Heidelberg D-69117, Germany.

‡Chemistry Department, Brookhaven National Laboratory, Upton, NY 11973-5000.

§Present address: Advanced Light Source, LBNL, Berkeley, CA 94720.

‖Present address: IBM Almaden Research Center, San Jose, CA 95120.

[1] See, for example, *Colossal Magnetoresistive Oxides*, edited by Y. Tokura (Gordon and Breach, New York, 2000).

[2] J. M. D. Coey, M. Viret, and S. von Molnar, Adv. Phys. **48**, 167 (1999).

[3] A. P. Ramirez, J. Phys.: Condens. Matter **9**, 8171 (1999).

[4] M. B. Salomon and M. Jaime, Rev. Mod. Phys. **73**, 583 (2001).

[5] E. Dagotto, *Nanoscale Phase Separation and Magnetoresistance* (Springer, New York, 2002).

[6] S. Jin, M. McCormack, T. H. Tiefel, and R. Ramesh, J. Appl. Phys. **76**, 6929 (1994).

[7] W. E. Pickett and D. J. Singh, Phys. Rev. B **53**, 1146 (1996).

[8] J.-H. Park, E. Vescovo, H.-J. Kim, C. Kwon, R. Ramesh, and T. Venkatesan, Nature (London) **392**, 794 (1998).

[9] J. Y. T. Wei, J. Appl. Phys. **83**, 7366 (1998).

[10] M. Bowen, M. Bibes, A. Barthelemy, J.-P. Contour, A. Anane, Y. Lemaitre, and A. Fert, Appl. Phys. Lett. **82**, 233 (2003).

[11] C. Zener, Phys. Rev. **82**, 403 (1951).

[12] A. J. Millis, P. B. Littlewood, and B. I. Shraiman, Phys. Rev. Lett. **74**, 5144 (1995).

[13] A. J. Millis, B. I. Shraiman, and R. Mueller, Phys. Rev. Lett. **77**, 175 (1996).

[14] J. M. De Teresa, M. R. Ibarra, P. A. Algarabel, C. Ritter, C. Marquina, J. Blasco, J. García, A. del Moral, and Z. Arnold, Nature (London) **386**, 256 (1997).

[15] C. H. Booth, F. Bridges, G. H. Kwei, J. M. Lawrence, A. L. Cornelius, and J. J. Neumeier, Phys. Rev. B **57**, 10440 (1998).

[16] D. Louca, T. Egami, E. L. Brosha, H. Roder, and A. R. Bishop, Phys. Rev. B **56**, R8475 (1997).

[17] Y. Murakami, H. Kawada, H. Kawata, M. Tanaka, T. Arima, Y. Moritomo, and Y. Tokura, Phys. Rev. Lett. **80**, 1932 (1998).

[18] A. Moreo, S. Yunoki, and E. Dagotto, Science **283**, 2034 (1999).

[19] N. Mathur and P. Littlewood, Phys. Today **56**(1), 25 (2003).

[20] N. Mannella, A. Rosenhahn, C. H. Booth, S. Marchesini, B. S. Mun, S. H. Yang, K. Ibrahim, Y. Tomioka, and C. S. Fadley, Phys. Rev. Lett. **92**, 166401 (2004).

[21] N. Mannella, A. Rosenhahn, M. Watanabe, B. Sell, A. Nambu, S. Ritchey, E. Arenholz, A. Young, Y. Tomioka, and C. S. Fadley, Phys. Rev. B **71**, 125117 (2005).

[22] N. Furukawa, Proceedings of the Workshop on Physics of Manganites, Michigan State University, July 1998, edited by T. A. Kaplan and S. D. Mahanti (Plenum, New York, 1998), available at arXiv:cond-mat/9812066v1 (1998).

[23] T. Okuda, A. Asamitsu, Y. Tomioka, T. Kimura, Y. Taguchi, and Y. Tokura, Phys. Rev. Lett. **81**, 3203 (1998); **81**, 3203 (1998).

[24] M. C. Martin, G. Shirane, Y. Endoh, K. Hirota, Y. Moritomo, and Y. Tokura, Phys. Rev. B **53**, 14285 (1996).

[25] E. Dagotto, T. Hotta, and A. Moreo, Phys. Rep. **344**, 1 (2001).

[26] D. Louca and T. Egami, J. Appl. Phys. **81**, 5484 (1997).

[27] D. Louca and T. Egami, Phys. Rev. B **59**, 6193 (1999).

[28] S. J. Hibble, S. P. Cooper, A. C. Hannon, I. D. Fawcett, and M. Greenblatt, J. Phys.: Condens. Matter **11**, 9221 (1999).

[29] A. Mellergard, R. L. McGreevy, and S. G. Eriksson, J. Phys.: Condens. Matter **12**, 4975 (2000).

[30] Y. Moritomo, A. Asamitsu, and Y. Tokura, Phys. Rev. B **56**, 12190 (1997).

[31] A. Urushibara, Y. Moritomo, T. Arima, A. Asamitsu, G. Kido, and Y. Tokura, Phys. Rev. B **51**, 14103 (1995).

[32] C. S. Fadley, M. A. VanHove, Z. Hussain, and A. P. Kaduwela, J. Electron Spectrosc. Relat. Phenom. **75**, 273 (1995).

[33] A. T. Young, V. Martynov, and H. A. Padmore, J. Electron Spectrosc. Relat. Phenom. **101-103**, 885 (1999).

[34] C. S. Fadley, in *Advances in Surface and Interface Science*, edited by R. Z. Bachrach (Plenum, New York, 1992).

[35] (a) J. Choi, C. Walfried, S.-H. Liu, and P. A. Dowben, J. Vac. Sci. Technol. A **16**, 2950 (1998); (b) J. Choi, J. Zhang, S.-H. Liou, P. A. Dowben, and E. W. Plummer, Phys. Rev. B **59**, 13453 (1999); (c) H. Dulli, P. A. Dowben, S.-H. Liou, and E. W. Plummer, *ibid.* **62**, 014629 (2000); (d) H. Dulli, E. W. Plummer, P. A. Dowben, J. Choi, and S.-H. Liu, Appl. Phys. Lett. **77**, 570 (2000); (e) M. P. de Jong, V. A. Dediu, C. Taliani, and W. R. Salanec, J. Appl. Phys. **94**, 7292 (2003); (f) M. P. de Jong, I. Bergenti, V. A. Dediu, M. Fahlman, M. Marsi, and C. Taliani, Phys. Rev. B **71**, 014434 (2005).

[36] A. W. Kay, F. J. Garcia de Abajo, S.-H. Yang, E. Arenholz, B. S. Mun, N. Mannella, Z. Hussain, M. A. Van Hove, and C. S. Fadley, Phys. Rev. B **63**, 115119 (2001); N. Mannella, S. Marchesini, A. W. Kay, A. Nambu, T. Gresch, S.-H. Yang, B. S. Mun, J. M. Bussat, A. Rosenhahn, and C. S. Fadley, J. Electron Spectrosc. Relat. Phenom. **141**, 45 (2004).

[37] J. J. Bucher, P. G. Allen, N. M. Edelstein, D. K. Shuh, N. W. Madden, C. Cork, P. Luke, D. Pehl, and D. Malone, Rev. Sci. Instrum. **67**, 3361 (1996).

[38] P. Eisemberger and G. S. Brown, Solid State Commun. **29**, 481 (1979).

[39] C. S. Fadley, D. A. Shirley, A. J. Freeman, P. S. Bagus, and J. V. Mallow, Phys. Rev. Lett. **23**, 1397 (1969).

[40] G. H. Gweon, J. G. Park, and S. J. Oh, Phys. Rev. B **48**, 7825 (1993).

[41] L. Sangaletti, L. E. Depero, P. S. Bagus, and F. Parmigiani, Chem. Phys. Lett. **245**, 463 (1995).

[42] T. Saitoh, A. E. Bocquet, T. Mizokawa, H. Namatame, A. Fujimori, M. Abbate, Y. Takeda, and M. Takano, Phys. Rev. B **51**, 13942 (1995).

[43] V. R. Galakhov, M. Demeter, S. Bartkowski, M. Neumann, N. A. Ovechkina, E. Z. Kurmaev, N. I. Lobachevskaya, Y. M. Mukowskii, J. Mitchell, and D. L. Ederer, Phys. Rev. B **65**, 113102 (2002), and references therein.

[44] B. Sinkovic, B. Hermsmeier, and C. S. Fadley, Phys. Rev. Lett. **55**, 1227 (1985).

[45] N. Mannella, A. Rosenhahn, A. Nambu, B. C. Sell, B. S. Mun, S. H. Yang, S. Marchesini, M. Watanabe, K. Ibrahim, S. B. Ritchey, Y. Tomioka, and C. S. Fadley, J. Electron Spectrosc. Relat. Phenom. **153**, 37 (2006).

[46] B. D. Hermsmeier, C. S. Fadley, B. Sinkovic, M. O. Krause, J. Jimenez-Mier, P. Gerard, T. A. Carlson, S. T. Manson, and S. K. Bhattacharya, Phys. Rev. B **48**, 12425 (1993).

[47] H. Nylen, Ph.D. thesis, Uppsala University, 1998.

[48] T. Saitoh, A. E. Bocquet, T. Mizokawa, H. Namatame, A. Fujimori, M. Abbate, Y. Takeda, and M. Takano, Phys. Rev. B **51**,

13942 (1995); J. H. Park, C. T. Chen, S. W. Cheong, W. Bao, G. Meigs, V. Chakarian, and Y. U. Idzerda, Phys. Rev. Lett. **76**, 4215 (1996); J. S. Kang, C. G. Olson, J. H. Jung, S. T. Lee, T. W. Noh, and B. I. Min, Phys. Rev. B **60**, 13257 (1999).

[49] R. Liu, W. C. Tonjes, C. G. Olson, J. J. Joyce, A. J. Arko, J. J. Neumeier, J. F. Mitchell, and H. Zheng, J. Appl. Phys. **88**, 786 (2000).

[50] G. Banach and W. M. Temmerman, Phys. Rev. B **69**, 054427 (2004).

[51] J. J. Lander, Phys. Rev. **91**, 1382 (1953).

[52] M. Cini, Solid State Commun. **20**, 605 (1976); G. A. Sawatzky, Phys. Rev. Lett. **39** 504 (1977); M. Cini, Phys. Rev. B **17**, 2788 (1978).

[53] P. A. Bennett, J. C. Fuggle, F. U. Hillebrecht, A. Lenselink, and G. A. Sawatzky, Phys. Rev. B **27**, 2194 (1983), and references therein.

[54] A. Sekiyama, S. Suga, M. Fujikawa, S. Imada, T. Iwasaki, K. Matsuda, T. Matsushita, K. V. Kaznacheyev, A. Fujimori, H. Kuwahara, and Y. Tokura, Phys. Rev. B **59**, 15528 (1999).

[55] A. Chainani, M. Mathew, and D. D. Sarma, Phys. Rev. B **47**, 15397 (1993).

[56] C. S. Fadley, in *Electron Spectroscopy, Theory, Techniques, and Applications*, edited by C. R. Brundle and A. D. Baker (Pergamon, New York, 1978), Vol. 2, Chap. 1.

[57] In order to complete the measurements within the time allowed in a single beamtime, it was not possible for the higher-energy experiment to change the temperature in steps as low as 20 K, resulting in different temperature steps and time constants.

[58] F. Offi, N. Mannella, T. Pardini, G. Panaccione, A. Fondacaro, P. Torelli, M. W. West, J. W. Mitchell, and C. S. Fadley, Phys. Rev. B (to be published).

[59] K. Horiba, M. Taguchi, A. Chainani, Y. Takata, E. Ikenaga, D. Miwa, Y. Nishino, K. Tamasaku, M. Awaji, A. Takeuchi, M. Yabashi, H. Namatame, M. Taniguchi, H. Kumigashira, M. Oshima, M. Lippmaa, M. Kawasaki, H. Koinuma, K. Kobayashi, T. Ishikawa, and S. Shin, Phys. Rev. Lett. **93**, 236401 (2004).

[60] H. Tanaka, Y. Takata, K. Horiba, M. Taguchi, A. Chainani, S. Shin, D. Miwa, K. Tamasaku, Y. Nishino, T. Ishikawa, E. Ikenaga, M. Awaji, A. Takeuchi, T. Kawai, and K. Kobayashi, Phys. Rev. B **73**, 094403 (2006).

[61] M. van Veenendaal, Phys. Rev. B **74**, 085118 (2006).

[62] Temperature-dependent XAS data on related compounds as well as a theoretical model for the correlation between the occurrence of local JTD and the presence or absence of the oxygen prepeak have been reported by O. Toulemonde, F. Millange, F. Studer, B. Raveau, J.-H. Park, and C.-T. Chen, J. Phys.: Condens. Matter **11**, 109 (1999).

[63] M. Abbate, F. M. F. de Groot, J. C. Fuggle, A. Fujimori, O. Strebel, F. Lopez, M. Domke, G. Kaindl, G. A. Sawatzky, M. Takano, Y. Takeda, H. Eisaki, and S. Uchida, Phys. Rev. B **46**, 4511 (1992).

[64] J.-H. Park, T. Kimura, and Y. Tokura, Phys. Rev. B **58**, R13330 (1998).

[65] E. D. Crozier, J. J. Rehr, and R. Ingalls, in *X-ray Absorption: Principles, Applications and Techniques of EXAFS, SEXAFS, and XANES*, edited by D. Konigsberger and D. Prins (Wiley, New York, 1988), p. 373; G. B. Beni and P. M. Platzman, Phys. Rev. B **14**, 1514 (1976).

[66] T. Shibata, B. A. Bunker, and J. F. Mitchell, Phys. Rev. B **68**, 024103 (2003).

[67] See, for example, A. S. Alexandrov and S. N. Mott, *Polarons and Bipolarons* (World Scientific, Singapore, 1995); A. S. Alexandrov and J. Ranninger, Phys. Rev. B **45**, 13109(R) (1992); S. Fratini and S. Ciuchi, Phys. Rev. Lett. **91**, 256403 (2003); S. Ciuchi, F. dePasquale, S. Fratini, and D. Feinberg, Phys. Rev. B **56**, 4494 (1997).

[68] M. Mayr, A. Moreo, J. A. Verges, J. Arispe, A. Feiguin, and E. Dagotto, Phys. Rev. Lett. **86**, 135 (2001).

[69] J. Burgy, M. Mayr, V. Martin-Mayor, A. Moreo, and E. Dagotto, Phys. Rev. Lett. **87**, 277202 (2001).

[70] T. Shibata, B. Bunker, J. F. Mitchell, and P. Schiffer, Phys. Rev. Lett. **88**, 207205 (2002).

[71] J. M. De Teresa, M. R. Ibarra, P. Algarabel, L. Morellon, B. Garcia-Landa, C. Marquina, C. Ritter, A. Maignan, C. Martin, B. Raveau, A. Kurbakov, and V. Trounov, Phys. Rev. B **65**, 100403(R) (2002).

[72] C. M. Varma, Phys. Rev. B **54**, 7328 (1996).

[73] P. S. Anil Kumar, P. A. Joy, and S. K. Date, J. Phys.: Condens. Matter **10**, L269 (1998).

[74] H. Yi, N. H. Hur, and J. Yu, Phys. Rev. B **61**, 9501 (2000).

[75] N. W. Aschroft and N. Mermin, *Solid State Physics* (Saunders College, Philadelphia, 1976), p. 656.